

Single-cell RNA sequencing reveals PDFGR α ⁺ stromal cell subpopulations that promote proacinar cell differentiation in embryonic salivary gland organoids

Nicholas Moskwa^{1,2,*}, Ayma Mahmood¹, Deirdre A. Nelson¹, Amber L. Altrieth^{1,2,3}, Paolo E. Forni^{1,2,3} and Melinda Larsen^{1,2,3,‡}

ABSTRACT

Stromal cells can direct the differentiation of epithelial progenitor cells during organ development. Fibroblast growth factor (FGF) signaling is essential for submandibular salivary gland development. Through stromal fibroblast cells, FGF2 can indirectly regulate proacinar cell differentiation in organoids, but the mechanisms are not understood. We performed single-cell RNA-sequencing and identified multiple stromal cell subsets, including *Pdgfra*⁺ stromal subsets expressing both *Fgf2* and *Fgf10*. When combined with epithelial progenitor cells in organoids, magnetic-activated cell-sorted PDGFR α ⁺ cells promoted proacinar cell differentiation similarly to total stroma. Gene expression analysis revealed that FGF2 increased the expression of multiple stromal genes, including *Bmp2* and *Bmp7*. Both BMP2 and BMP7 synergized with FGF2, stimulating proacinar cell differentiation but not branching. However, stromal cells grown without FGF2 did not support proacinar organoid differentiation and instead differentiated into myofibroblasts. In organoids, TGF β 1 treatment stimulated myofibroblast differentiation and inhibited the proacinar cell differentiation of epithelial progenitor cells. Conversely, FGF2 reversed the effects of TGF β 1. We also demonstrated that adult salivary stromal cells were FGF2 responsive and could promote proacinar cell differentiation. These FGF2 signaling pathways may have applications in future regenerative therapies.

KEY WORDS: FGF2, Myofibroblast, Mouse organoid, PDGFR α , Stroma, Submandibular salivary gland

INTRODUCTION

All developmental processes require precise cellular organization and coordination between many cell types. Branching morphogenesis in the parenchymal epithelium of salivary glands requires instructions from embryonic mesenchymal or adult stromal cells (Sakakura et al., 1976; Wei et al., 2007). These stromal-to-epithelial interactions shape epithelial differentiation, instructing

either secretory acinar or ductal cell fates. Functional salivary acini produce saliva and promote good oral health (Pedersen et al., 2018). However, acinar cells accumulate damage from diseases, such as type 2 diabetes and Sjögren's syndrome, from oral drug use, and from radiotherapy for head and neck cancer (Jensen et al., 2014; Liu et al., 2012; Marmary et al., 2016; Plemons et al., 2014; von Bültzingslöwen et al., 2007; Weng et al., 2018; Yoo et al., 2014). Improved therapeutics for diseased and dysfunctional salivary glands require characterization of the molecular mechanisms involved in stromal-epithelial cell interactions that drive secretory acinar cell differentiation.


Tissue recombination experiments first demonstrated that mesenchymal cells in salivary glands impact epithelial differentiation (Hoffman, 2002; Kusakabe et al., 1985; Sakakura et al., 1976; Wei et al., 2007). Fibroblast growth factor (FGF) signaling mediates important stromal epithelial interactions, which facilitate developmental processes, including limb formation and wound healing (De Moerloose et al., 2000; Martin, 1998). FGF signaling between the stroma and epithelium also affects how submandibular salivary glands (SMGs) develop (Chatzeli et al., 2017; Hoffman, 2002; Lombaert et al., 2013; Makarenkova et al., 2009; Steinberg et al., 2005; Wei et al., 2007). The FGF growth factor family is a large and complex family, with 23 known interacting members and four receptors with multiple isoforms (Yun et al., 2010). Mice with FGFR2IIIb knocked out exhibit abnormal salivary gland development (De Moerloose et al., 2000; Ohuchi et al., 2000) because the epithelium ignores stromal signals. Similarly, when the FGFR2IIIb receptor ligand, FGF10, is knocked out, early gland development fails (Tina Jaskoll et al., 2005; Ohuchi et al., 2000; Steinberg et al., 2005). The salivary gland connective tissue includes diverse cell types, such as stromal fibroblasts, vascular endothelial cells and nerves, which synergize for instructing development (Kwon et al., 2017; Nedvetsky et al., 2014; Takebe et al., 2013, 2015). In previous work, we formed complex salivary organoids from embryonic day (E) 16 epithelial and stromal cells, which underwent robust FGF2-dependent proacinar cell differentiation (Hosseini et al., 2018, 2019). FGFR pharmacological inhibition or FGF2 knockdown specifically within the stroma inhibited epithelial proacinar cell differentiation. However, stromal factors that directly promote epithelial proacinar cell differentiation were not identified.

Using hierarchical clustering, single-cell RNA-sequencing (scRNA-Seq) has revealed high levels of cellular heterogeneity within organs (Enge et al., 2017; Hauser et al., 2020; Kwon et al., 2019; Lu et al., 2016; Macosko et al., 2015; McCarthy et al., 2020b; Sekiguchi et al., 2020; Song et al., 2018; Zepp et al., 2017, 2021). These large datasets and their computational models have identified diverse cell subsets within known cell types. This

¹Department of Biological Sciences, University at Albany, State University of New York, Albany, NY 12222, USA. ²Graduate Program in Molecular, Cellular, Developmental and Neural Biology, University at Albany, State University of New York, Albany, NY 12222, USA. ³The RNA Institute, University at Albany, State University of New York, Albany, NY 12222, USA.

*Present address: The Jackson Laboratory, Farmington, CT 06032, USA.

‡Author for correspondence (mlarsen@albany.edu)

 N.M., 0000-0002-9819-9227; A.M., 0000-0002-5287-3183; D.A.N., 0000-0001-5527-2570; A.L.A., 0000-0002-1107-0077; P.E.F., 0000-0001-6547-3464; M.L., 0000-0002-5026-2012

extra complexity in known cellular communications increases developmental nuances and reveals previously uncharacterized cellular specificities. In this study, we identified numerous stromal cell subpopulations in both E16 SMG and complex salivary organoids using scRNA-Seq. Moreover, using microarray and scRNA-Seq, we determined that FGF2 directly regulates the stromal cell phenotype. We identified effects of FGF2-dependent stromal BMP genes on epithelial proacinar cell differentiation. *Pdgfra* is a FGF2-controlled gene that is expressed in several stromal subpopulations in the salivary gland. PDGFR α ⁺ stromal cells alone sufficiently promoted epithelial proacinar cell differentiation in salivary organoids. FGF2-dependent BMP genes synergized with FGF2, promoting proacinar cell differentiation. FGF2 sustained stromal competence that instructed epithelial proacinar cell differentiation, prevented stromal myofibroblast transition in culture and reversed TGF β 1-mediated proacinar cell dedifferentiation in organoid cultures.

RESULTS

ScRNA-Seq identification of multiple salivary gland stromal cell subpopulations

Given that our previous research showed that proacinar cell differentiation in our complex salivary organoids required E16 SMG stromal cells (Hosseini et al., 2018), we hypothesized that specific stromal subpopulations may direct epithelial proacinar cell differentiation. We addressed this hypothesis by performing scRNA-Seq using enriched stromal cells isolated from E16 SMGs. The compiled scRNA-Seq data contained 9165 fully sequenced cells (Fig. S1). The transcriptional subpopulations were modeled using Seurat's principal component analysis (PCA) followed by k-nearest neighbor clustering and Louvain algorithms (Satija et al., 2015). We visualized the modeled subpopulations using graph-based dimensional Uniform Manifold Approximation and Projection (UMAP) reductions. Based on cells expressing the gene encoding epithelial cell adhesion molecule (*Epcam*), we sequenced 1195 epithelial cells and 7970 nonepithelial cells (Fig. 1A). Epithelial cell segregation and reanalysis (Fig. 1C) yielded nine epithelial subpopulations, including known epithelial subtypes, such as *Krt5*⁺ and *Krt19*⁺ ductal cells and *Epcam*⁺*Acta2*⁺ myoepithelial cells (Hauser et al., 2020; Song et al., 2018). Additionally, we found that the two distinct proacinar populations expressing either *Smgc* or *Bpifa2*, previously reported in postnatal day (P) 1 SMG (Hauser et al., 2020), were detectable at E16. We also identified many connective tissue cell types (Fig. 1A,B; Fig. S1). Based on *Coll1a1* expression, we sequenced 3790 stromal fibroblast cells. The remaining 4180 cells included endothelial cells, lymphatic endothelial cells, immune cells, neurons, Schwann cells and erythrocytes, as defined by marker gene expression.

The stromal fibroblasts were segregated and reclustered, identifying 13 previously undefined stromal cell subpopulations (Fig. 1D). Nine subpopulations are classifiable based on the known stromal identity markers *Pdgfra*, *Pdgfrb*, *Acta2*, *Thy1* and *Wnt2* (Contreras et al., 2019; Dominici et al., 2006; Karpus et al., 2019; Kishi et al., 2018; Li et al., 2018; Santini et al., 2020; Zepp et al., 2017, 2021), and proliferative subpopulations accounted for the other four stromal clusters. Both PDGFR α and PDGFR β are especially interesting because cells expressing these receptors have been shown to play important roles in organ epithelial differentiation, wound healing and disease phenotypes (Kinchen et al., 2018; Kramann et al., 2015; Kuppe et al., 2021; Li et al., 2018; Liu et al., 2019; Ramachandran et al., 2019; Santini et al., 2020). PDGFR α is expressed in the neural crest-derived SMG

mesenchyme, and PDGF signaling regulates early branching morphogenesis through FGFs (Hoffman, 2002; Morikawa et al., 2009; Sakakura et al., 1976; Soriano, 1997; Steinberg et al., 2005; Yamamoto et al., 2008). We annotated the transcriptomes of the *Pdgfra*⁺ subpopulations using Metascape (Zhou et al., 2019) and found transcriptional landscapes matching the traditionally understood functions of the stroma. These *Pdgfra*⁺ clusters showed differing Gene Ontology (GO) categories for extracellular matrix organization, vasculature development and supramolecular fiber organization (Fig. 1E). We evaluated subpopulations expressing two growth factors with known importance in proacinar cell differentiation: *Fgf2* (Hosseini et al., 2018) and *Fgf10* (Chatzeli et al., 2021; Patel et al., 2007; Wells et al., 2013) (Fig. 1F). Of the nine *Pdgfra*⁺ subclusters, seven expressed *Fgf2* and *Fgf10* at varying levels, suggesting that these stromal subpopulations may participate in proacinar cell differentiation instruction.

To explore the possible developmental relationship between heterogeneous stromal cell types, we modeled cell differentiation trajectories in pseudotime (Fig. 1G). Using Monocle DDRTree (Qiu et al., 2017), we inferred trajectories from the E16 scRNA-Seq transcriptomes. We set the root node as the noncell-cycling *Pdgfra*⁺ subpopulation because previous reports indicated that the stroma arises from the *Pdgfra*⁺ migratory cranial neural crest (Morikawa et al., 2009). The resulting trajectory analysis showed three branches: one branch directly linked the *Pdgfra*⁺ root subpopulation with the *Wnt2*⁺*Thy1*⁺ subpopulation; a second branch led to another *Pdgfra*⁺ subpopulation that expresses more ECM genes compared with the root population; and a third branch transitioned from a *Pdgfra*⁺ state through the cell cycle into a *Pdgfrb*⁺*Acta2*⁺ subpopulation. This analysis predicts that the *Pdgfra*⁺ progenitor population has multiple differentiation trajectories during SMG development.

FGF2 promotes proacinar cell differentiation while inhibiting ductal differentiation

Given that organoids can be used to evaluate stromal-epithelial cell signaling, we examined the changes in salivary gland organoid epithelial gene expression in response to FGF2. We produced organoids containing E16 SMG epithelial and stromal cells grown with or without FGF2, as performed previously (Hosseini et al., 2018, 2019). We separated the organoid epithelial cells from the stromal cells and identified epithelial differentiation transcriptomes using microarrays. We detected a clear separation between the control- and FGF2-treated epithelial cells in the first principal component (PC1) of the PCA (Fig. S2C). We generated a twofold change heatmap and noted specific acinar and ductal differentiation markers showing contrasting signal magnitudes between the FGF2 and control conditions (Fig. 2A). FGF2 increased proacinar gene expression, as expected based on our prior work (Hosseini et al., 2018, 2019), including known proacinar genes, *Smgc* [encoding mucin 19 (MUC19)] and *Bpifa2* [encoding parotid secretory protein (PSP)], and known acinar genes that are not highly expressed at the protein level at E16, including *Proll* [encoding mucin 10 (MUC10)] and *Bhlha15* [encoding muscle, intestine and stomach expression 1 (MIST1)]. Gene set enrichment analysis (GSEA) (Subramanian et al., 2005), using gene sets derived from P8 SMG epithelial scRNA-Seq data (Song et al., 2018), identified global differences showing acinar and ductal genes enriched under FGF2-cultured and control conditions, respectively (Fig. 2B). However, neither organoid condition showed myoepithelial gene enrichment. Using immunocytochemistry (ICC), we confirmed

Fig. 1. scRNA-Seq shows distinct stromal subpopulations in E16 SMGs. (A) Seurat-generated UMAP plot using scRNA-Seq data from enriched stromal E16 SMGs. Supervised clustering and gene expression instructed cell type labeling. All expected major cell types were present. (B) Dot plot showing two marker genes per cell type and their corresponding expression levels. Gene expression informed cell cluster labeling. (C,D) UMAP and violin plots generated by (C) subsetting epithelial data and (D) subsetting stromal data. Epithelial segregation and reclustering showed the predicted epithelial subtypes, labeled with cell type and markers. Newly defined stromal cell subpopulations are labeled by marker expression. Pa, *Pdgfra*; Pb, *Pdgfrb*; CC, cell cycle. (E) Metascape analysis of nonproliferative *Pdgfra*⁺ stromal cells. Stromal segregation and reclustering revealed novel stromal cell subpopulations. (F) Dot plot of stromal gene expression only, showing a correlation of *Pdgfra* with *Fgf2* and *Fgf10* expression (red boxes). (G) Stromal subset data interpreted using pseudotime modeling. *Pdgfra*⁺*Pdgfrb*⁺ cells were chosen as the root node (indicated by '1'). This differentiation projection shows *Pdgfra*⁺*Pdgfrb*⁺ cell progression through cell cycle (solid black lines) to reach an *Acta2*⁺ state, then either directly progressing to a *Thy1*⁺ state, or progressing to a *Pdgfra*⁺ state and producing relatively more extracellular matrix.

that, in organoids lacking FGF2, expression of the ductal marker KRT7 progressively increased and was inversely correlated with the acinar marker, AQP5 (Fig. S2A,B). Together, these results identify an FGF2-dependent proacinar transcriptome, and an emerging ductal transcriptome if FGF2 is absent.

Stromal cells are required for myoepithelial cell differentiation independently of FGF2

Given that *in vivo* SMGs contain both proacinar cells and adjacent myoepithelial cells, forming bilayered acini, we looked for protein-level evidence that FGF2 regulates myoepithelial cell differentiation. Organoids were grown for 7 days with or without stroma and with or without FGF2, and ICC was performed with the myoepithelial marker, calponin 1 (CNN1). When stroma was present, CNN1 was detected in the organoids, whereas stroma-deficient organoids had little-to-no detectable CNN1. Stromal cell-containing organoids showed similar CNN1 levels, independent of FGF2 (Fig. 2C,D), consistent with transcriptional analysis. To confirm that CNN1 was expressed by myoepithelial cells, we grew epithelial-stromal organoids with and without FGF2 and performed ICC using CNN1 together with the epithelial marker, EPCAM, and the basement-membrane protein heparan sulfate proteoglycan 2 (HSPG2 or perlecan). With high-magnification confocal imaging, we confirmed that the EPCAM⁺ cells expressing CNN1 were enclosed within the HSPG2⁺ basement membrane (Fig. 2E), as expected in myoepithelial cells. These data demonstrate that, without FGF2 signaling, stromal cells can sufficiently stimulate myoepithelial cell differentiation.

FGF2 sustains stromal cell populations in organoids that mirror cell populations *in vivo*

Given that we had previously determined that stromal cells are the direct targets of FGF2 signaling in salivary gland organoids (Hosseini et al., 2018), we evaluated the effects of FGF2 on the stromal cell phenotype. Isolated E16 stromal cells were grown on glass coverslips or on porous polycarbonate filters in the presence or absence of FGF2. Stromal cells grown on glass with FGF2 showed a different cellular morphology compared with cells grown without FGF2. Although the PDGFR β area was constant, there was a threefold increase in area in cultured cells expressing PDGFR α in the presence of FGF2 (Fig. 3A,B). Additionally, THY1 expression was generally elevated in stromal cells grown with FGF2 on glass (Fig. S3A,B). Thus, the organization of the stroma was dependent

on the culture surface but not on FGF2. Although the stromal cells grew as a 2D monolayer on glass, they coalesced into 3D spherical aggregates when cultured on the filters, reminiscent of mesenchymal stem cells in a classical colony-forming assay (Friedenstein et al., 1970). Additionally, stromal cells grown on softer polycarbonate filters with FGF2 showed a threefold increase in relative cell area that was positive for THY1 (Fig. 3C,D). In organoids treated with or without FGF2, FGF2-dependent PDGFR α , and FGF2-independent PDGFR β expression in stroma was consistent with that in the 2D cultures (Fig. 3E,F). Thus, stromal cell PDGFR α and THY1 protein levels are dependent on FGF2 signaling. To examine these cell populations *in vivo*, we performed immunohistochemistry on E16 and adult SMG tissue sections and identified key stromal markers: PDGFR α , PDGFR β , vimentin (VIM), ENG and THY1 (Fig. 3G). We detected stromal cell subpopulations expressing markers generally comparable with the scRNA-Seq profile of the E16 gland (Fig. 1C). scRNA-Seq showed a small *Thy1*⁺ stromal subpopulation that was also *Wnt2*⁺ and *Pdgfra*⁺ (Fig. 1D). Interestingly, in tissue sections, these THY1⁺ stromal cells resided in a neurovasculature region near endothelial cells expressing platelet endothelial cell adhesion molecule (PECAM1/CD31) and neuronal cells expressing tubulin- β 3 (TUBB3) in the adult SMG (Fig. 3G).

Although we previously reported that total E16 stromal cells can promote proacinar cell differentiation in adult epithelial cells in organoids (Koslow et al., 2019), we did not examine whether adult stromal cells can instruct proacinar cell differentiation in our complex salivary organoids. We tested this by isolating and expanding adult stromal cells in FGF2-containing media. Once enough stromal cells formed, they were combined into organoids using E16 SMG epithelial cells. Significantly, expanded adult SMG stromal cells retained PDGFR α expression and, based on AQP5 expression, promoted epithelial proacinar cell differentiation (Fig. 3H,I). These data indicate that adult stromal cells can instruct FGF2-dependent proacinar cell differentiation.

PDGFR α ⁺ stromal cells are sufficient to direct epithelial proacinar cell differentiation in salivary organoids

We next questioned whether PDGFR α ⁺ stromal fibroblasts sufficiently promote proacinar cell differentiation in organoids. We isolated E16 PDGFR α ⁺ stromal cells using magnetic-activated cell sorting (MACS). We compared organoids generated using MACS PDGFR α ⁺-selected cells with organoids containing epithelial cells alone or epithelial cells with whole E16 stroma. Organoids containing only epithelial cells and treated with FGF2 demonstrated little to no PDGFR α ⁺ stromal cell contamination (Fig. 4A,B), very low expression of AQP5 and no budding (Fig. 4C, D). By contrast, organoids formed using PDGFR α ⁺ MACS-sorted stroma or total stroma showed a similar PDGFR α ⁺ area (Fig. 4A,B). Significantly, these FGF2-treated organoids containing MACS-isolated PDGFR α ⁺ stromal cells showed high AQP5 expression and branched morphology comparable with whole stroma-containing organoids (Fig. 4C,D). These data demonstrate that PDGFR α ⁺ stromal cells are sufficient to stimulate the budding proacinar organoid phenotype.

FGF2-stimulated stromal cells induce proacinar cell differentiation in organoids using BMPs

To identify how FGF2 stimulation changes the transcriptome of SMG stromal cells and instructs epithelial proacinar cell differentiation, we performed scRNA-Seq analysis on enriched stromal cells derived from organoids in the presence or the absence

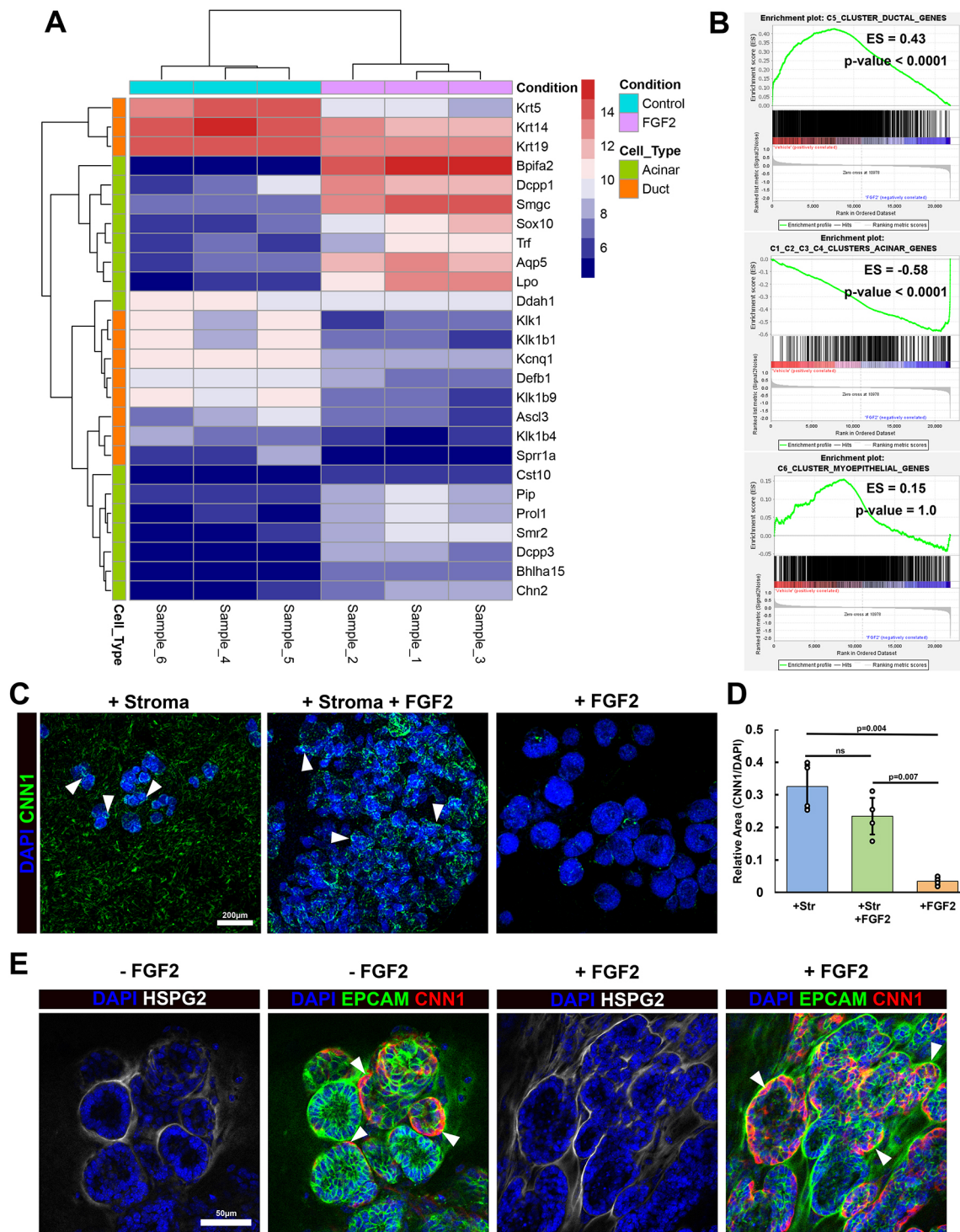


Fig. 2. Proacinar, ductal and myoepithelial phenotypes are controlled in salivary gland organoids by FGF2 and stroma. (A) Transcriptome heatmap showing enrichment of specific acinar (green) and ductal (salmon-pink) genes with FGF2 (purple) and control (cyan) organoid culture conditions, respectively. A log twofold scale for microarray signals is shown in red (higher) and blue (lower). (B) GSEA plots depicting microarray differential gene enrichment across ductal, acinar and myoepithelial gene lists. Plots show that FGF2-cultured organoids were enriched for acinar genes, whereas control organoids were enriched in ductal genes. Neither organoid was enriched for myoepithelial genes. Enrichment scores (ESs) and nominal *P*-values are provided. (C) E16 SMG organoids grown with or without stroma and with or without exogenous FGF2 immunostained to detect CNN1 (green) with the nuclear stain DAPI (blue). Only organoids grown with stromal cells contained CNN1⁺ epithelium (arrowheads). (D) Quantification of organoid area positive for CNN1 normalized to DAPI. Organoids formed from stroma had significantly more myoepithelium; data are mean±s.d.; *n*=4 technical replicates (single-factor ANOVA with post-hoc Tukey test). (E) Immunostained E16 SMG epithelial and stromal cell-containing organoids cultured with and without FGF2. An EPCAM⁺ (green) and CNN1⁺ (red) myoepithelial layer was present within the epithelial compartment, surrounded by an HSPG2⁺ (white) basement membrane (arrowheads) both in the presence and absence of FGF2. Nuclei stained with DAPI (blue).

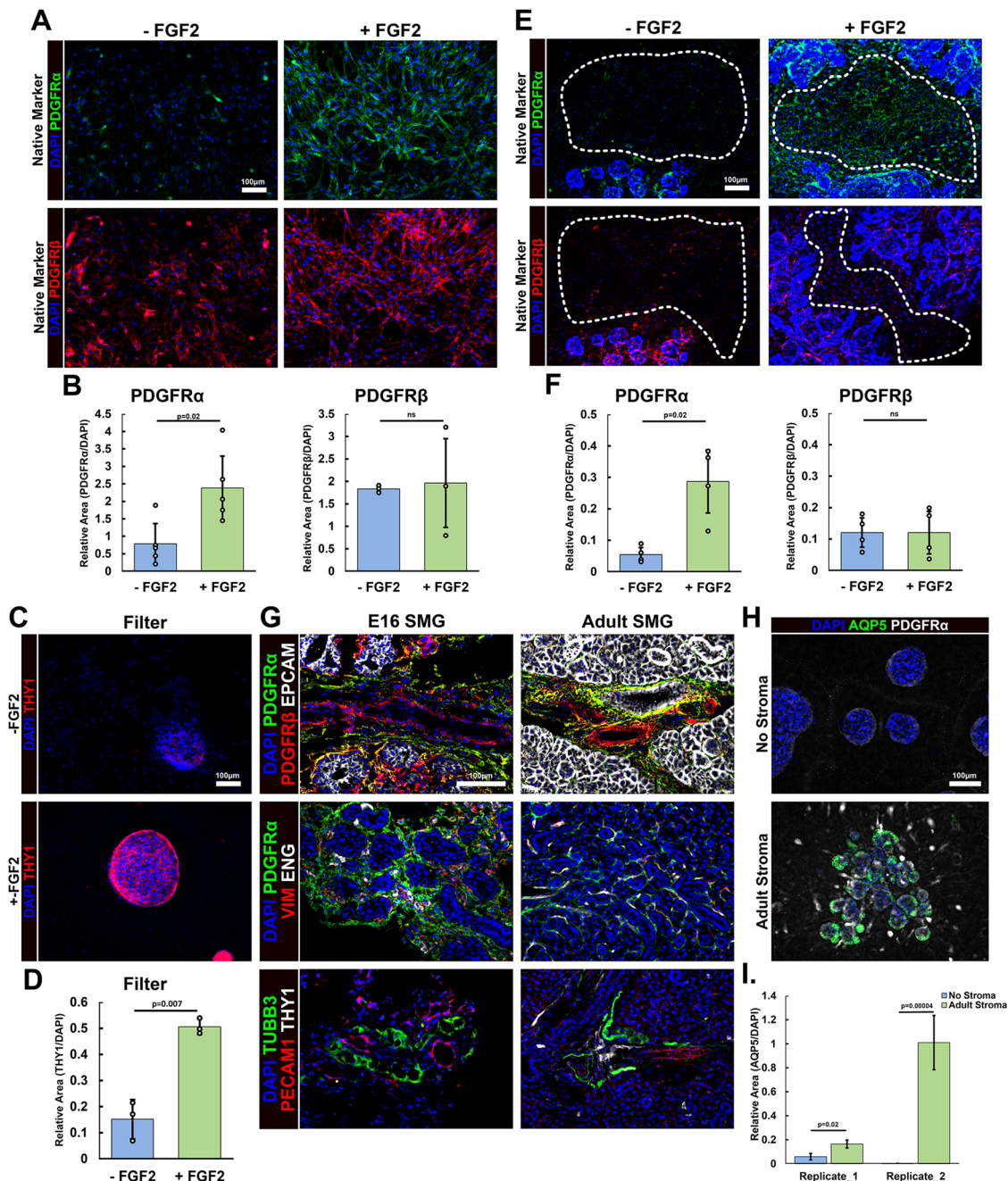


Fig. 3. SMG stromal cells cultured with exogenous FGF2 retain an *in vivo*-like phenotype. (A) E16 stromal cells cultured on coverslips in medium with or without FGF2. Cells positive for PDGFR α (green) and PDGFR β (red) increased when exogenous FGF2 was present, shown by DAPI staining (blue). (B) Cell area quantification of PDGFR α and PDGFR β normalized to DAPI area. FGF2 increased the stromal PDGFR α -positive area threefold but did not affect the PDGFR β -positive area significantly; data are mean \pm s.d.; $n=5$ and 3 experimental replicates, respectively (two-tailed unpaired Student's t -test). (C) E16 stroma cultured on porous filters in media with or without FGF2 with ICC performed to detect THY1 (red), with nuclei stained with DAPI (blue). On filters, FGF2 signaling increased E16 stromal THY1 expression. (D) Area stain quantification of THY1 normalized to DAPI, showing a statistically relevant threefold increase in THY1 expression; data are mean \pm s.d.; $n=4$ and 3 technical replicates (two-tailed unpaired Student's t -test). (E) Changes in stromal gene expression in the organoids. ICC was performed on E16 SMG epithelial and stromal organoids cultured with or without FGF2-containing medium. PDGFR α (green) and PDGFR β (red) staining showed similar responses in organoids to those in stromal-only cultures. Only PDGFR α was increased in organoid stroma (dashed white lines) when FGF2 was present. PDGFR β remained unchanged in either condition. (F) Area stain quantification within organoids. The PDGFR α /DAPI-positive area increased fivefold in organoid stroma when FGF2 was added. The PDGFR β /DAPI-positive area did not change in organoid stroma; data are mean \pm s.d.; $n=4$ technical replicates (two-tailed unpaired Student's t -test). (G) Immunostaining for stromal markers performed on E16 and adult salivary gland cryosections. Both PDGFR α (green) and PDGFR β (red) were expressed in E16 and adult SMGs, with single- and dual-positive cells detected. Other stromal markers, VIM (red) and ENG (white), were also expressed in PDGFR α ⁺ stromal cells. A rare stromal subset expressing THY1 (white) occurred near neuronal TUBB3⁺ (green) and endothelial PECAM⁺ (red) cells within a presumptive neural-vascular niche. Nuclei are labeled using DAPI (blue). (H) Organoids created using E16 epithelium cultured in FGF2 media either with or without cultured adult stroma. ICC showed proacinar epithelium using AQP5 (green) and DAPI (blue). The adult stroma supported proacinar epithelium, similar to that seen with total E16 stroma. PDGFR α ⁺ (white) stroma was present in organoids containing adult stroma. (I) AQP5-positive area quantified relative to epithelial cell DAPI. The organoids cultured with adult stroma showed a significantly increased AQP5 relative area compared with organoids cultured without stroma; data are mean \pm s.d.; Replicate_1=4 and Replicate_2=7 technical replicates (two-tailed unpaired Student's t -test).

of FGF2. After Seurat analysis, we detected multiple cell types, including the expected stromal enrichment in both datasets (Fig. 5A, B; Fig. S4). When both datasets were integrated, a significant shift was seen in the presence (yesFGF2) or absence (noFGF2) of FGF2 (Fig. 5C,D). The stroma of the FGF2 organoid contained a high percentage of cells expressing both *Pdgfra* and *Thy1* (Fig. 5E,F). Both genes were predominantly in clusters 0, 1, 6 and 8, and showed GO categories associated with cell movement and vasculature development (Fig. 5G). The stromal subpopulations in control organoids lacking FGF2 contained higher numbers of cells expressing *Acta2* and/or *Pdgfrb* (Fig. 5E,F). These clusters were labeled as 2, 3, 7 and 10, and were enriched for GO categories of actin cytoskeletal arrangement, cell adhesion, vascular development, response to wounding and ECM organization (Fig. 5G).

Using microarrays, we also examined the transcriptomic changes in organoid stromal cells depending on the presence or absence of FGF2. PC1 of the PCA accounted for over 50% of the variance and demonstrated significant differences between the two conditions (Fig. 6A). We examined comprehensive transcriptomic changes that were FGF2 dependent using GSEA (Subramanian et al., 2005) and observed that FGF2 treatment enriched many stromal gene sets associated with proliferation or targets of the proliferation-inducing E2F transcription factors (Fig. 6B). Gene enrichment of E2F targets was expected because FGF2 participates in driving the cell cycle (Krejci et al., 2004; Neary et al., 2005).

To identify FGF2-regulated paracrine factors that may instruct epithelial proacinar cell differentiation, we targeted the growth factors that were differentially expressed. From this list, we selected three growth factor genes with a greater than twofold difference in expression with and without FGF2: amphiregulin (*Areg*), epiregulin (*Ereg*), and bone morphogenetic protein 7 (*Bmp7*) (Fig. 6C). These three growth factors were also upregulated in scRNA-Seq-described subpopulations from the FGF2 organoid stroma (Fig. 6D). Prior research illustrated the mixed contributions of BMPs to promoting salivary gland branching morphogenesis (Hoffman, 2002; Steinberg et al., 2005), but epithelial cell differentiation was not addressed. However, in intestinal organoids, hair follicles and lungs, BMPs induce epithelial cell differentiation (Lu et al., 2016; McCarthy et al., 2020a; Zepp et al., 2017). *Areg* and *Ereg* are EGF homologs, and EGF signaling is a known SMG developmental promoter (Mizukoshi et al., 2016). We tested whether any of these three factors could substitute for the stroma. We created epithelial organoids lacking stroma but cultured with media containing FGF2 and one candidate growth factor. BMP7, but neither EGF family ligand (AREG or EREG) induced AQP5 in conjunction with FGF2 (Fig. 6E,F), although budding of the organoid decreased. We validated that BMP signaling in the epithelium is necessary for proacinar marker expression using a BMP inhibitor. Epithelial-only organoids were treated with FGF2, BMP7 and a selective BMP receptor inhibitor, LDN19318, which targets primarily ALK2 and ALK3. Combined treatment with FGF2, BMP7 and LDN19318 resulted in no proacinar marker expression in the epithelial organoids, which looked similar to FGF2-only cultured organoids (Fig. 6G,H). Given that BMP2 is another BMP family member that can signal through ALK2 and ALK3 (Sanchez-Duffhues et al., 2020) and was FGF2-dependently upregulated in both the microarray and scRNA-Seq (Fig. 6C,D; Fig. S4), we also tested BMP2 in FGF2-treated epithelial organoids. The response to BMP2 was similar to that to BMP7, synergizing with FGF2 and promoting AQP5 expression (Fig. 6I,J). Thus, these data identify BMP signaling as a FGF2-

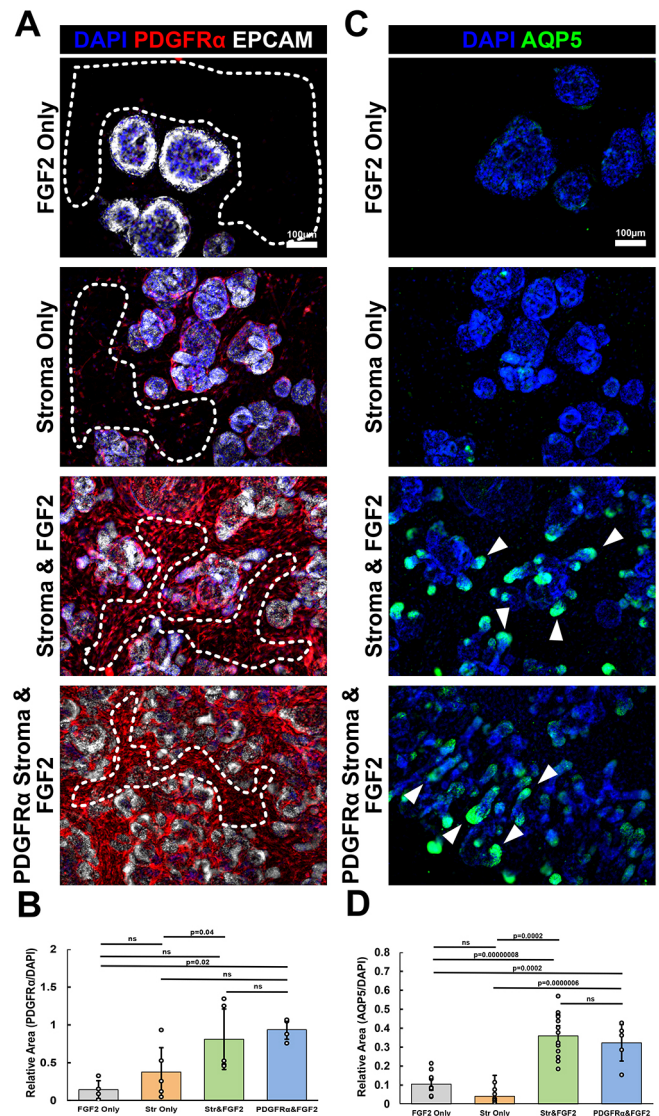


Fig. 4. MACS-selected PDGFR α ⁺ stromal cells induce proacinar organoids. (A) E16 organoids created using epithelium cultured with: FGF2 and no stroma (FGF2 Only); stroma without FGF2 (Stroma Only); stroma and FGF2 (Stroma & FGF2); or with PDGFR α ⁺ MACS-isolated stromal cells and FGF2 (PDGFR α Stroma & FGF2). ICC for EPCAM (white) shows the epithelium, PDGFR α ⁺ (red) shows the stromal subsets and DAPI (blue) shows the nuclei. Although all conditions formed epithelial organoids, stromal PDGFR α only increased when FGF2 was present. Dashed white outlines indicate stromal regions. (B) The PDGFR α -positive area was quantified relative to stromal cell DAPI area. PDGFR α ⁺ MACS-selected stroma showed a greater than twofold increase in PDGFR α , similar to the total stroma when FGF2 was present; data are mean \pm s.d.; $n=4, 5, 5$ and 4 experimental replicates, respectively (single-factor ANOVA with post-hoc Tukey test). (C) E16 organoids created using epithelium cultured with: FGF2 and no stroma (FGF2 Only); stroma without FGF2 (Stroma Only); stroma and FGF2 (Stroma & FGF2); or with PDGFR α ⁺ MACS-isolated stroma and FGF2 (PDGFR α ⁺ Stroma & FGF2). ICC for AQP5 (green) shows the proacinar epithelium and DAPI (blue) shows the nuclei. AQP5 increased equally when either total stroma or PDGFR α ⁺ stroma was combined with FGF2. Arrowheads indicate epithelial areas with robust AQP5 expression. (D) The AQP5-positive area was quantified relative to DAPI. AQP5 increased when either total stroma or PDGFR α ⁺ stroma was in the presence of FGF2-containing media; data are mean \pm s.d.; $n=11, 9, 14$ and 5 experimental replicates, respectively (single-factor ANOVA with post-hoc Tukey test).

dependent, stromal-produced, paracrine-acting pathway that promotes proacinar cell differentiation in salivary organoids through FGF2 synergy.

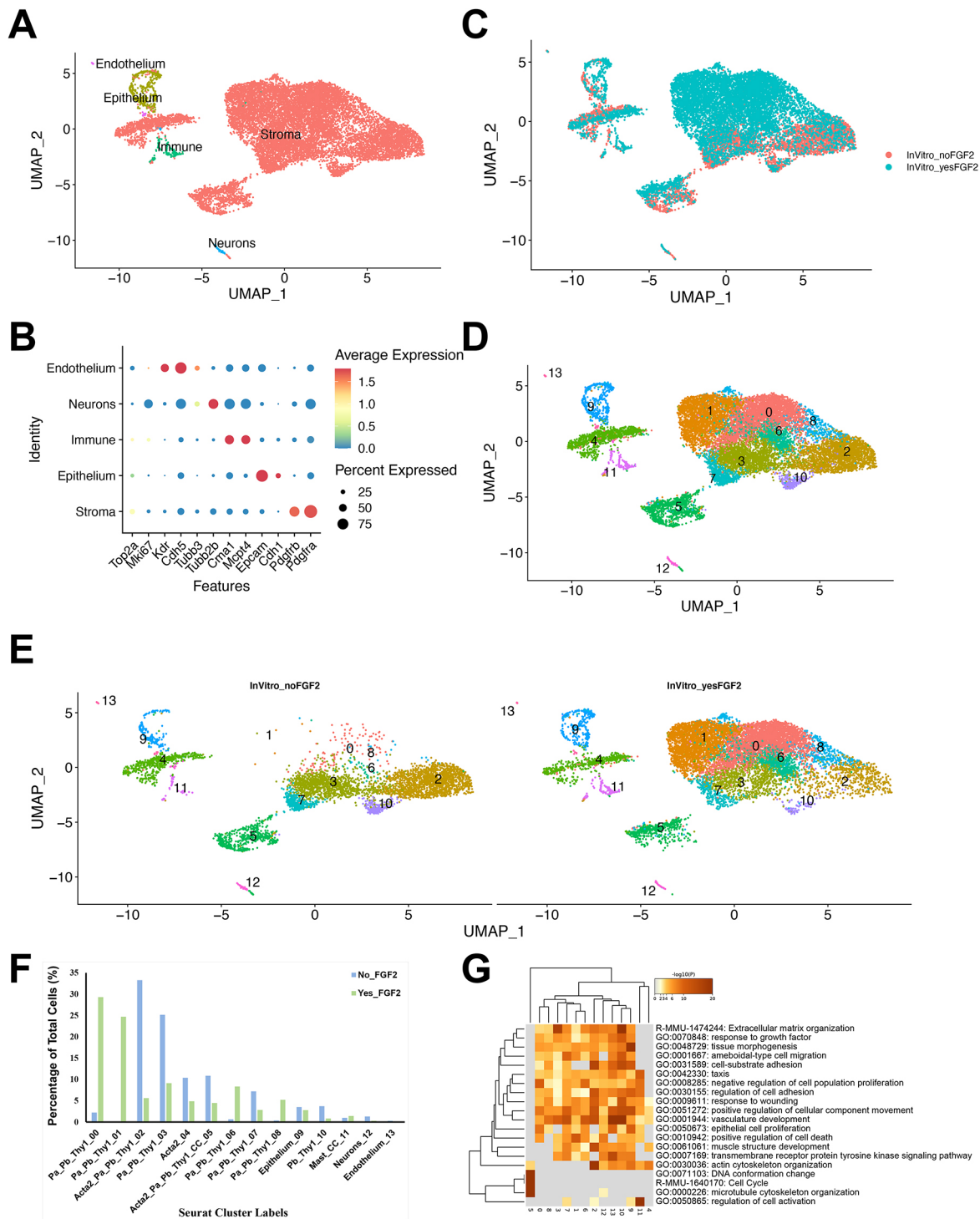


Fig. 5. Organoid scRNA-Seq shows that FGF2 modulates specific stromal subpopulations. (A) Seurat-generated UMAP plot integrating scRNA-Seq data from organoids grown with or without FGF2 enriched for stroma. Supervised clustering and gene expression instructed cell type labeling. The data demonstrate effective stromal enrichment. (B) Dot plot showing marker gene per cell type with the percentage of cells expressing each marker and their corresponding expression levels. Gene expression informed cell cluster labeling. (C) UMAP colored based on cells from FGF2+ (InVitro_yesFGF2, Cyan) or FGF2– (InVitro_noFGF2, Salmon) samples. The data demonstrate effective stromal enrichment. (D) UMAP clusters derived from the k-nearest neighbor algorithm. Multiple stromal cell subclusters are revealed. (E) UMAPs separated based on sample organoid. Clusters 0, 1, 6 and 8 were enriched with FGF2+ stroma, whereas clusters 2, 3, 7 and 10 were enriched with FGF2– stroma. (F) Bar graphs showing cell percentages for each cluster from each sample. (G) Metascape analysis of all stromal clusters showing differential enhancement of pathway activation in stromal cell subclusters.

FGF2 inhibits and reverses myofibroblast differentiation in salivary gland organoids

Based on the increased *Acta2* and *Cnn1* expression in the stroma and reduced PDGFR α staining in organoids when FGF2 was

absent, we questioned whether lacking FGF2 phenotypically changes stromal cells. We examined the microarray gene sets enriched in the stroma grown without FGF2 (Fig. 7A). Three of the most significantly enriched gene sets, identified by GSEA, were

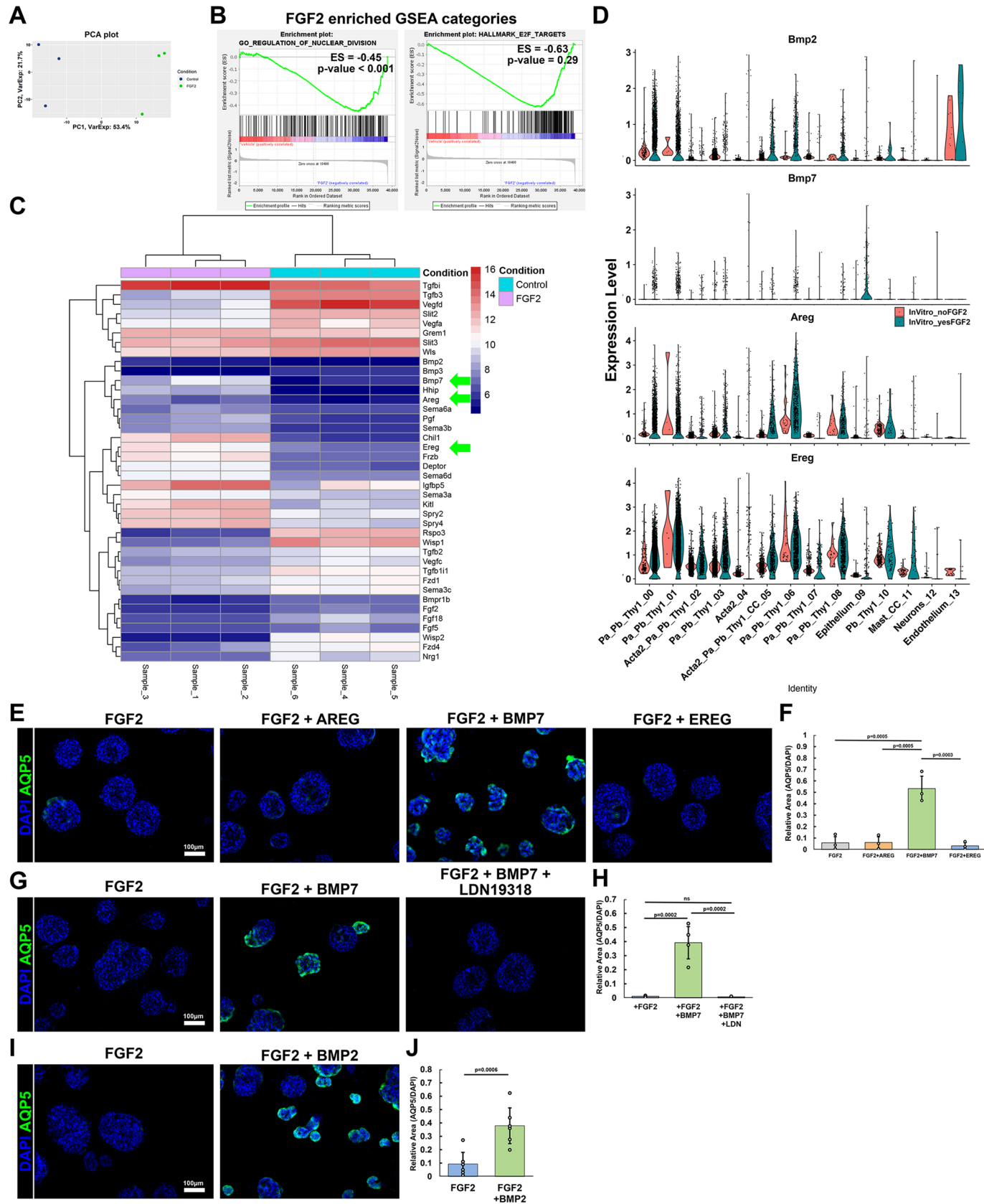


Fig. 6. See next page for legend.

Fig. 6. FGF2-dependent BMP signaling promotes epithelial proacinar cell differentiation. (A) PCA plot comparing Clariom-D microarray data generated from organoid stroma grown with or without FGF2. Each point represents one experimental replicate. More than half of the variance was described by PC1; $n=3$ experimental replicates. (B) Enriched GSEA charts for microarray transcriptomes from E16 organoid stroma cultured with or without FGF2. Many stromal-enriched genes were associated with cell division. Enrichment score (ES) and nominal P -values are provided. (C) Heatmap showing secreted factor changes in organoid stroma grown with or without FGF2. Growth factors selected for further analysis are indicated by green arrows. (D) E16 scRNA-Seq violin plots for stromal microarray genes. Of the growth factors selected for further analysis, only *Bmp7* transcription was detected in E16 stromal subsets. (E) ICC in epithelial-only organoids cultured with FGF2 and either AREG, BMP7, or EREG, plus AQP5 (green) and DAPI (blue). (F) Epithelial organoid area positive for AQP5 normalized to DAPI. FGF2- and BMP7-cultured organoids showed a significant tenfold increase in relative AQP5-stained area compared with organoids cultured with only FGF2; data are mean \pm s.d.; $n=3$ experimental replicates (single-factor ANOVA with post-hoc Tukey test). (G) ICC in epithelial-only organoids cultured with FGF2 alone or in conjunction with either BMP7 or BMP7+LDN19318, plus AQP5 (green) with DAPI (blue). (H) Epithelial organoid area positive for AQP5 normalized to DAPI. LDN19318 significantly reduced the AQP5-relative area of organoids 40-fold; data are mean \pm s.d.; $n=4$ experimental replicates (single-factor ANOVA with post-hoc Tukey test). (I) ICC in organoids created using only E16 epithelium grown with media containing FGF2 or FGF2+BMP2 plus AQP5 (green) and DAPI (blue). BMP2, in combination with FGF2, promoted AQP5 expression. (J) Epithelial organoid area positive for AQP5 normalized to DAPI. FGF2-and-BMP2-cultured organoids showed a significant fourfold increase in relative stained area compared with FGF2-only cultured organoids; data are mean \pm s.d.; $n=6$ experimental replicates (single-factor ANOVA with post-hoc Tukey test).

myogenesis, extracellular matrix and TGF β signaling. All three gene sets align with myofibroblast characteristics. We hypothesized that, without FGF2, stromal cells differentiate into myofibroblasts. Myofibroblasts are known injury and fibrotic disease contributors that increase extracellular matrix deposition (Contreras et al., 2019; Kramann et al., 2015; Kuppe et al., 2021; Li et al., 2018; Nagaraju et al., 2019). We generated a heatmap for core myofibroblast genes that showed that all genes were more highly expressed in control organoid stroma compared with FGF2-treated organoid stroma (Fig. 7B). Based on the *in vivo* scRNA-Seq trajectory prediction (Fig. 1F, Fig. 7C) and organoid scRNA-Seq data (Fig. 5, Fig. 7D; Fig. S4), E16 stromal cells have the differentiation potential to express the classical myofibroblast gene smooth muscle alpha actin (α SMA) and TGF β ligands. We used GSEA to determine which scRNA-Seq-described SMG subpopulation best represented the transcriptome of the total control organoid stroma (Fig. 7E), finding that the *Pdgfrb*⁺*Acta2*⁺, stromal cluster 10 (SC_10), genes were most representative. These data suggest that the SC_10 transcriptome dominates control organoid stroma and has myofibroblast-like characteristics.

To confirm whether SMG stromal cells differentiate into a myofibroblast-like state in the absence of FGF2, we cultured E16 stromal cells alone on coverslips with or without FGF2 and performed ICC using classical myofibroblast markers. Stromal cells grown without FGF2 showed a nearly fivefold elevation in the myofibroblast markers, α SMA and CNN1, relative to cells grown with FGF2 (Fig. 7F,G). To determine whether similar changes in gene expression occurred in the organoids, we examined α SMA and CNN1 expression in organoids grown with or without FGF2. We detected a similar myofibroblast-like transition in organoids in the absence of FGF2, but only with a threefold change (Fig. 7H,I). A time-course was performed with time points at 2, 4 and 7 days to examine explicitly myofibroblast conversion in organoids in the absence of FGF2. At day 2, there was no significant difference in CNN1 staining in the organoid stroma relative to FGF2 treatment

(Fig. 7J,K). By day 4, there was noticeably more myofibroblast marker expression in the control organoid stroma, and this myofibroblast marker expression increased into day 7. These data support the hypothesis that SMG stromal cells progressively differentiate into a myofibroblast-like state in the absence of FGF2.

Two mRNAs that were increased in organoid stroma grown without FGF2 (no_FGF2) were *Tgfb2* and *Tgfb3* (Fig. 7B), which are TGF β family profibrotic cytokines that can induce myofibroblast differentiation and fibrosis (Avery et al., 2018; Nagaraju et al., 2019; Ó Hainmhire et al., 2019; Woods et al., 2015). Notably, the *Acta2*⁺*Pdgfrb*⁺ stromal cluster (SC_10) showed appreciable *Tgfb2* and *Tgfb3* expression in the scRNA-Seq-defined stromal cell subsets (Fig. 7C). Both Tgf β s were also upregulated in specific organoid stromal subpopulations in control conditions (Fig. 7D). We tested TGF β signaling in the organoids by treating them either for 4 days with TGF β and subsequently with FGF2 for 3 days (Fig. S5A,B) or with FGF2 for 4 days and subsequently with TGF β for 3 days (Fig. S5C,D). These experiments showed a correlation between proacinar inhibition and the myofibroblast phenotype, revealing an inherent plasticity in both the epithelial and stromal cell populations (Fig. S5). We also found that prolonged culturing, for up to seven passages, increased CNN1 expression in the stroma, indicative of a myofibroblast phenotype. These late-passage stromal cells did not promote proacinar cell differentiation when incorporated into FGF2-treated organoids (Fig. S6A,B). We further tested whether TGF β signaling inhibits proacinar cell differentiation. First, organoid AQP5 expression was induced after culturing with FGF2 for 5 days. Then, FGF2 was washed out and replaced with TGF β 1-containing media. One day after TGF β 1 addition, the area positive for the proacinar marker, AQP5, had decreased threefold (Fig. 7L,M). Notably, this TGF β 1-induced AQP5 reduction was reversible after TGF β 1 media was washed away and FGF2 media was reapplied. AQP5 re-expression occurred 4 days after FGF2 re-introduction (Fig. 7L). These FGF2-TGF β 1-FGF2 sequentially cultured organoids had AQP5 staining similar to that in organoids grown with FGF2 for 10 consecutive days (Fig. 7M). Together, these data indicate that TGF β treatment inhibits proacinar organoid differentiation in a reversible fashion and that FGF2 can reverse TGF β 1-mediated proacinar inhibition. This epithelial reversal occurs after the myofibroblast-like phenotype in the stroma reverses.

DISCUSSION

Even though it has been known for decades that stromal fibroblasts direct organ development, recent advances in scRNA-Seq are illuminating the specific contributions of this diverse population. Here, we performed scRNA-Seq on developing salivary glands and organoids and evaluated the contributions of stromal cell subpopulations to acinar cell differentiation. We defined subpopulations using specific markers describing functional stromal subsets in other organs, specifically *Pdgfra*, *Pdgfrb*, *Acta2*, *Eng*, *Thy1* and *Wnt2* (Karpus et al., 2019; Kramann et al., 2015; Kwon et al., 2019; Lee et al., 2017; Li et al., 2018; Santini et al., 2020; Stzepourginski et al., 2017; Yang et al., 2017; Zepp et al., 2021; Zhao et al., 2017). Our pseudotime analysis interpretation suggests that these burgeoning subpopulations arise from a *Pdgfra*⁺ population that differentiates into multiple subpopulations. Organoid stromal scRNA-Seq provides evidence that these divergent differentiating stromal cells are FGF2 dependent. UMAP regression and superimposed pseudotime models revealed that these stromal cells progress through a continuous transcriptional landscape rather than by discrete

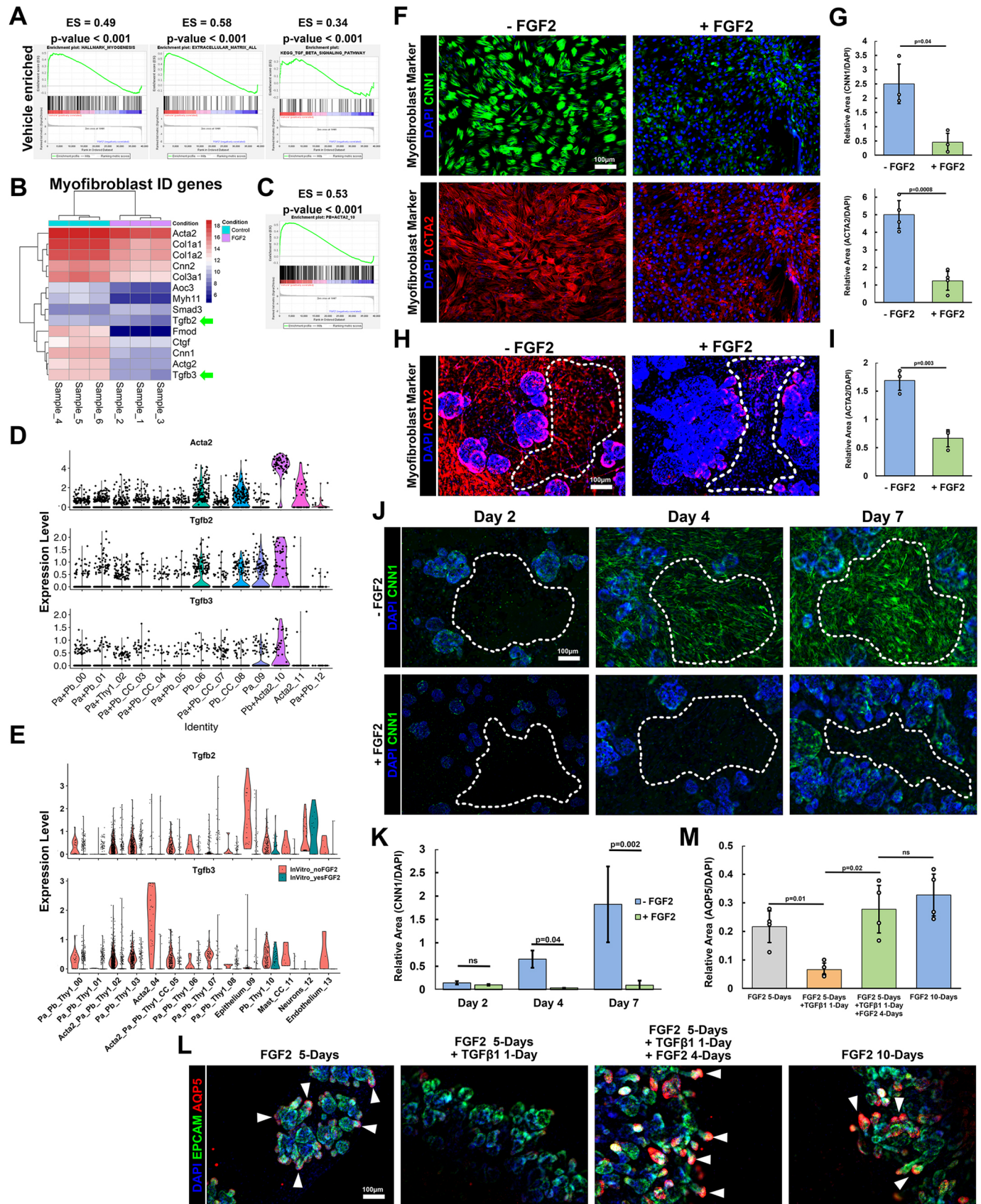


Fig. 7. See next page for legend.

Fig. 7. E16 stromal cells cultured with exogenous FGF2 resist an inhibitory myofibroblast differentiation. (A) E16 organoid stroma transcriptomes showing myofibroblast-enriched gene sets in control conditions. Enrichment score (ES) and nominal *P*-values are provided. (B) Heatmap showing classical myofibroblast genes, including *Acta2*, *Cnn1*, *Tgfb2* and *Tgfb3*, were higher in E16 organoid stroma under control than under FGF2 conditions. Growth factors selected for further analysis are indicated by green arrows. (C) GSEA plot showing that the gene expression of E16 control organoid stroma was similar to the *in vivo* smooth muscle cell phenotype described by the scRNA-Seq data (cluster 10, E16). ES and nominal *P*-values are provided. (D) *Acta2*, *Tgfb2* and *Tgfb3* violin plots from E16 SMG stromal scRNA-Seq data. (E) *Tgfb2* and *Tgfb3* violin plots from E16 organoid stromal scRNA-Seq data cultured with or without FGF2. (F) E16 stroma cultured on coverslips in the presence or absence of FGF2. Immunostaining showed that both myofibroblast markers CNN1 (green) and ACTA2 (red) increased when the cells were cultured without FGF2. (G) Quantification of the myofibroblast marker area normalized to the DAPI area, showing a fivefold increase in ACTA2 and CNN1, in no-FGF2 cultured stroma; data are mean \pm s.d.; *n*=3 and 4 experimental replicates, respectively (two-tailed unpaired Student's *t*-test). (H) E16 epithelial and stromal organoids cultured with or without FGF2. The ACTA2 signal (red) was higher in stroma without FGF2. The dashed white outline shows stromal regions. (I) Quantification of ACTA2⁺ area normalized to stromal DAPI⁺ area. The ACTA2 signal was twofold higher in organoid stroma without FGF2; data are mean \pm s.d.; *n*=3 technical replicates (two-tailed unpaired Student's *t*-test). (J) E16 organoid developmental time-course on days 2, 4 and 7, using ICC for CNN1 (green). The stroma expressed increasing CNN1 over time. The dashed white outline shows stromal regions. (K) Quantification of CNN1 area normalized to DAPI area. The amount of CNN1 in stroma steadily increased as organoids were grown without FGF2; data are mean \pm s.d.; *n*=3 technical replicates (two-tailed unpaired Student's *t*-test). (L) E16 epithelium and stromal organoids grown over 5, 6 and 10 days. FGF2 medium was applied first for 5 days to prevent the myofibroblast phenotype and induce the proacinar phenotype. An additional 1 day of culture with TGF β simulated a myofibroblast response and decreased epithelial AQP5 (red) expression. Four days after FGF2 re-introduction, AQP5 levels were restored similar to those in organoids grown continuously with FGF2 for 10 days. Arrowheads indicate epithelial areas with robust AQP5 expression. (M) Area stain quantification. The 1-day TGF β introduction significantly reduced AQP5 normalized expression threefold relative to 5 days of treatment with FGF2. FGF2 re-introduction and culture restored AQP5 levels to match organoids cultured continuously for 10 days with FGF2; data are mean \pm s.d.; *n*=4 technical replicates (single-factor ANOVA with a post-hoc Tukey test).

trajectories. By contrast, other developmental scRNA-Seq data using pseudotime analysis suggest that embryonic epithelial subpopulations in the SMG and lung become more transcriptomically isolated over time (Hauser et al., 2020; Zepp et al., 2021). Whether stromal cells differentiate into distinct subpopulations, as epithelial populations do, is not yet firmly established. However, our data show a dualistic response to the growth factors FGF2 and TGF β 1 and suggest that stromal cells remain more plastic during development. Recent studies reveal that, in other organs, specific stromal subpopulations help create microniches that localize distinct epithelial identities into specific regions and mediate disease responses (Contreras et al., 2019; Li et al., 2018; McCarthy et al., 2020b; Santini et al., 2020; Yang et al., 2017). Similarly, we identified stromal cell subpopulations expressing *Pdgfra* that support proacinar cell differentiation in embryonic organoids (Fig. 8).

Our developmental model suggests that E16 stromal cells have multiple transcriptomic trajectories. The model predicts that these PDGFR α ⁺ cells can transition into two smaller subpopulations that increase either *Thy1* or *Acta2/Pdgfrb*. Our *in vitro* studies, in which stromal cells were cultured either with or without FGF2, showed that PDGFR α ⁺ cells can differentiate into at least two different subpopulations, which expressed markers analogous with the pseudotime subpopulations modeled as end nodes. This finding is

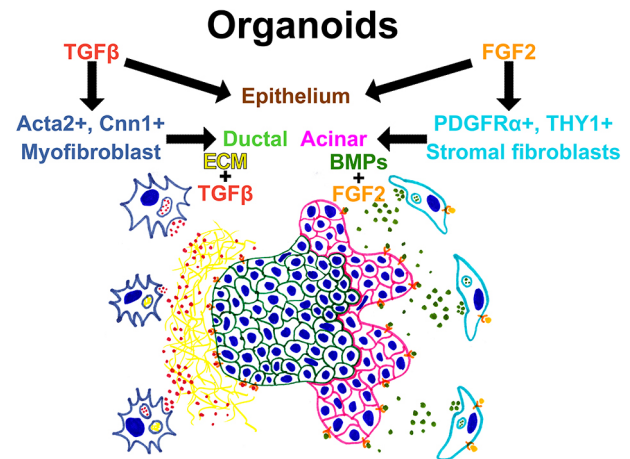


Fig. 8. Schematic model for FGF2-mediated stromal control of epithelial differentiation in embryonic salivary gland organoids. (A) FGF2 signaling causes *in vivo*-like stromal marker expression, including that of PDGFR α . The PDGFR α ⁺ stroma specifically produces BMPs, which promote proacinar cell differentiation and synergize with FGF2. Without FGF2, epithelial cells express ductal markers. TGF β ligands signal stromal differentiation into myofibroblasts. The myofibroblast phenotype and TGF β ligands, produced by both myofibroblasts and epithelial cells in the absence of FGF2, antagonize proacinar cell dedifferentiation.

consistent with that of others who have shown that PDGFR α ⁺ stromal cells have a transcriptomic plasticity that is important for regulating both developmental and injury responses (Contreras et al., 2019; Li et al., 2018). Using organoids, we explored the control of a specific stromal population over the epithelium, finding that FGF2 maintains a PDGFR α ⁺ stromal state resembling *in vivo* stromal cell gene expression. Cells in this stromal state can promote epithelial proacinar cell differentiation. We provide evidence that stromal cells expressing *Pdgfrb* and *Acta2* resemble classically defined myofibroblasts that do not support the proacinar cell differentiation state. The current definition of a myofibroblast is controversial and myofibroblasts have different characteristics *in vivo* and *in vitro* (Bochaton-Piallat et al., 2016). Whether *Pdgfra*⁺ cells become myofibroblasts is not clear and, in addition, how PDGFR α and PDGFR β signaling contributes to organoid differentiation also remains to be determined. Nevertheless, we have identified a clear relationship between the transcriptomic state of stromal cells and the differentiation state of salivary gland epithelial cells.

Others have suggested that PDGFR α stromal expression aligns with functional dexterity (Contreras et al., 2019; Li et al., 2018; Santini et al., 2020). Our organoid experiments showed that these PDGFR α ⁺ cells can recapitulate the function of the whole stroma in promoting proacinar cell differentiation. Organoids containing embryonic or adult stroma both retained similar proacinar-promoting abilities, which suggests a functional preservation in some stromal cell populations. The continuing instructiveness but decreasing cellular proportions of the stroma during development may reflect a conversion of the epithelium from stromal paracrine signaling to homeostatic autocrine signaling. As epithelial cells reach maturity, they may exhibit reduced stromal dependence in homeostasis and the stroma may no longer be required at high density unless damage occurs. Organoids can model damage and repair mechanisms and, thus, under these conditions, we showed that adult stromal cells can direct epithelial differentiation. Interestingly, the adult stroma retains FGF2 sensitivity and the

ability to promote proacinar cell differentiation when cultured with FGF2. Whether the mechanisms through which adult and E16 stromal cells induce proacinar cell differentiation are similar or whether adult cells that support proacinar cell differentiation are PDGFR α ⁺ remain to be determined.

Our study additionally suggests that the stromal state affects the differentiation of epithelial progenitor cells into ducts or acini (Fig. 8). First, FGF2 stimulates stromal PDGFR α and BMP expression. BMP signaling directs the epithelium toward a proacinar rather than a ductal state. However, BMPs are insufficient on their own to directly induce proacinar cell differentiation; FGF2 signaling is also required but is also insufficient. FGF2 signaling may somehow ‘prime’ the epithelium to respond to the BMP signal. Results of our organoid experiments, using only epithelial cells and growth factors, also indicated that proacinar cell differentiation and branching morphogenesis are distinct processes. This idea is in line with studies showing that BMP7 does not complement branching morphogenesis (Hoffman, 2002; Steinberg et al., 2005), and studies demonstrating that cell-to-matrix adhesions direct branching morphogenesis (Sakai et al., 2003; Wang et al., 2021). Other FGF-dependent and FGF-independent signaling pathways contribute to morphogenesis. Stromal BMPs directing epithelial differentiation is a theme in many organs. A similar BMP gradient induced by PDGFR α ⁺ cells also controls differentiation in the small intestinal crypt (McCarthy et al., 2020a). These intestinal PDGFR α ^{hi} telocytes and our PDGFR α ⁺ salivary stroma may be functionally and transcriptomically similar. This BMP shift contrasts with a second effect that FGF2 has in salivary organoids, whereby FGF2 signaling also prevents PDGFR α ⁺ cells from differentiating into ACTA2⁺/CNN1⁺ myofibroblasts. This myofibroblast phenotype produces at least one known branching morphogenesis-inhibiting growth factor, TGF β (Hall et al., 2010; Woods et al., 2015). TGF β inhibits proacinar cell differentiation and morphogenesis, and likely promotes ductal differentiation, as previously reported (Iwano et al., 2002; Liu et al., 2016; Rastaldi et al., 2002; Rees et al., 2006; Termén et al., 2013). This BMP and TGF β signaling axis may control the balance between developmental maturation and injury recovery. BMPs are known TGF β signaling antagonists, largely due to competition for shared intracellular signal transduction pathway mediators (Ning et al., 2019). TGF β is important for early salivary gland development (Jaskoll and Melnick, 1999) and is co-opted during injury for repurposing cells. The BMPs that originally differentiate cells during development (Bandyopadhyay et al., 2006; Lu et al., 2016; McCarthy et al., 2020a,b) can be used to redifferentiate adult cells post-injury. However, further time-dependent stromal analyses during injury will be needed to confirm this stromal switch.

Evaluating stromal heterogeneity remains a difficult frontier. Organs with smaller stromal cell proportions, such as salivary glands (Hauser et al., 2020), require cell enrichment steps before informative scRNA-Seq and hierarchical clustering can be performed. Even if the adult stromal population is small, our findings suggest that the adult stroma in salivary glands retains a therapeutic potential. However, more studies evaluating the evolution of stromal cell subpopulations at later developmental stages and additionally in disease models will be needed to effectively manipulate stromal cells for regenerative medicine approaches. Our research demonstrates the advantage of the organoid model for evaluating predictions made with scRNA-Seq. Organoids facilitate modular testing of cellular and mechanistic hypotheses that enable big data approaches, such as scRNA-Seq.

Overall, understanding the stromal complexity is necessary for understanding cellular interactions that could inspire useful regenerative therapies.

MATERIALS AND METHODS

Mouse submandibular gland cell isolation and enrichment

E16 timed-pregnant CD-1 female *Mus musculus* were ordered from Charles River Laboratories. First, the E16 embryos and then the SMGs from those embryos were dissected out following animal protocols approved by the University at Albany Institutional Animal Care and Use Committee (IACUC). SMG removal involved slicing the mandible with a sharp scalpel and then removing the glands using sterile forceps under a dissecting microscope (Nikon SNZ800). SMGs were microdissected in 2 \times collagenase/hyaluronidase (StemCell Technologies, 7912) diluted using 1 \times PBS (Life Technologies, 70011-044). The solution was further diluted, and SMGs were further dissected into lobules, when an additional volume of 1.6 U/ml of dispase II (Life Technologies, 17105041) was added, creating a final concentration of 0.8 U/ml dispase II. The lobules were further broken down after a 30-min incubation at 37°C followed by trituration, generating epithelial clusters and single stromal cells. Enzymatic activity was quenched with 10% fetal bovine serum (FBS) (Life Technologies, 10082147) in 1:1 DMEM/F12 (Life Technologies, 11039047) supplemented with 100 U/ml penicillin and 100 mg/ml streptomycin (Pen-Strep; Life Technologies, 15140122). Cell populations were separated by gravity sedimentation for ~10 min until the large clusters formed a loose pellet. Any DNA-induced clumping was stopped using 0.05 mg/ml DNase I (STEMCELL Technologies, 07900) during the second gravity sedimentation. The stromal cells were enriched by filtration of the resulting supernatant through 70 μ m (Falcon, 087712) and 40 μ m cell strainers (Thermo Fisher Scientific, 22363547). Filtered stroma were pelleted at 300 \times g for 8 min and the buffer was replaced using DMEM/F12 containing 10% FBS and Pen-Strep.

Epithelial clusters were enriched, as previously described (Hosseini et al., 2018, 2019), from the gravity pellet with two additional gravity sedimentations and by plating the clusters into a 35 mm tissue culture dish, incubating at 37°C for 2 h and then collecting the floating cells. Any suspended stromal cells were removed from epithelial clusters using two washes with centrifugation at 10 \times g for 1 min, supernatant removal and resuspension in medium.

E16 stroma scRNA-Seq

Stromal cells were enriched, as described above, from SMGs harvested from 14 E16 embryos. The embryos were excised from two CD-1 timed-pregnant female mice. Dead-cell depletion was performed using the Miltenyi dead-cell removal kit (Miltenyi Biotec, 130-090-101). The live-to-dead cell ratios and cell numbers were evaluated with Trypan Blue (Gibco, 15250-061) staining and a hemocytometer (Marienfeld Superior, Neubauer-improved). The preparation had >80% viable cells and was frozen down in cryovials using 90% FBS+10% dimethyl sulfoxide (Amresco, 200-664-3). Cells were frozen at -1°C/min in a 100% isopropanol freezing chamber overnight at -80°C. Frozen cells were stored in a liquid-nitrogen chamber prior to shipping overnight on dry ice. Cellular recovery goal for library preparation was 10,000 cells. scRNA library preps were created and sequenced by Singulomics or created in-house using the Chromium Next GEM Single Cell 3' GEM, Library & Gel Bead Kit v3.1 (10X Genomics, 1000121) and sequenced at the University at Albany Center for Functional Genomics.

Computational analysis of scRNA-Seq data

Bcl2fastq and Cell Ranger v4.0 were used to assemble and count the sequence data. Data files were imported using SEURAT v3.1.5 in R v3.6.3 (R Core Team, 2021) and R Studio v1.2.5042. Data clusters were calculated following the default pipeline (Satija et al., 2015; Stuart et al., 2019). Dead or apoptotic cells were removed if >7% of unique molecular identifiers (UMIs) mapped to mitochondrial genes. Any cells with <200 or >9000 genes were also removed before downstream analysis to remove noncells and doublets, respectively. The ‘ElbowPlot’ function and PC ‘Heatmaps’ helped determine how many PCs were used for unsupervised cluster

modeling. Clustering calculations used linear dimensional reduction, and visualization was performed using nonlinear dimensional reductions and UMAP. In total, 40 PCs were used for E16 stroma calculations, 21 PCs and 40 PCs were used for the epithelial subset and the stroma subset calculations, respectively and 20 PCs were used for the integrated organoid datasets.

The genes defining the unsupervised clustering were determined using the function ‘FindAllMarkers’. Visualization in R required library packages `cowplot v1`, `dplyr v0.8.5`, `ggplot2 v3.3.0`, `patchwork v1`, `magrittr v1.5` and `stringr v1.4`. Stromal subpopulation analysis in Metascape (Zhou et al., 2019) used all positively differentiated genes in the stromal clusters.

E16 and adult gland cryopreservation and sectioning

E16 and adult salivary glands were removed from CD-1 mice and preserved following a standard method (Shubin et al., 2017). Glands were fixed with 4% paraformaldehyde (PFA; Electron Microscopy Sciences, 15710) in 1×PBS for 2 h. The fixative was washed three times with 1×PBS. The glands were then dehydrated using three consecutive 1-h sucrose incubations at 4°C with 5%, 10% and 15% sucrose (Fisher, 57-50-1). Another two overnight incubations at 4°C were then performed first with 30% sucrose, then 15% sucrose and 50% Tissue Freezing Medium (TFM; Electron Microscopy Sciences, 72592). The fixed and dehydrated glands were frozen in TFM by floating the samples over liquid nitrogen. Cryosections were cut at 10 μm using a Leica CM1860 cryostat and adhered to charged histological slides (Electron Microscopy Sciences, 71869-10).

E16 PDGFR α ⁺ stromal cell isolation

Enriched E16 SMG stromal cells were pelleted at 300× *g* for 8 min. The media was removed and the stroma was resuspended in 90 μl FACS buffer [1×Hanks’ buffered saline solution (HBSS); Life Technologies, 14175095], 10% FBS and 5 mM EDTA (Falcon, S311-100), and positively selected using 10 μL PDGFR α antibody-coated microbeads (1:10; Miltenyi Biotec, 130-101-547). PDGFR α ⁺ stroma was placed into MACS immunomagnetic cell separation columns (Miltenyi Biotec, 130-042-021) and isolated following the manufacturer’s instructions. PDGFR α ⁺ stromal cells were pelleted at 300× *g* for 8 min, resuspended in 1 ml of media, and counted using a hemocytometer.

Organoid culture

Approximately 900 epithelial clusters (derived from one gland) grown with or without 20,000–50,000 stromal cells (derived from 0.2 glands) were embedded in Matrigel (Corning, 356234) at a 1:1 ratio to a total of 10 μl and seeded on 0.1 μm pore porous polycarbonate filters (Whatman Nuclepore, 0930051) floated on top of media in 50 mm glass-bottom dishes (MatTek P50G-1.5-14F). The cell preparations were incubated at 37°C in a tissue culture incubator (Thermo Fisher Scientific Forma Series II) with 5% CO₂ for 7 days to form organoids. Medium was replaced after incubating for 4 days. Media used in these experiments included DMEM/F12 with 10% FBS and Pen-Strep with growth factors or inhibitors added. Growth factors included: amphiregulin (AREG, 100 ng/ml; Peprotech, 315-36), BMP2 (100–200 ng/ml; Peprotech, 120-02), BMP7 (100–200 ng/ml; Peprotech, 120-03P), FGF2 (100 ng/ml; Peprotech, 450-33), EREG (100 ng/ml; Peprotech, 100-04) and TGF- β 1 (TGF β , 5 ng/ml; Peprotech, 100-12). Growth factors were solubilized in 0.2% bovine serum albumin (BSA; Sigma Millipore, A2934-100G) in water and stored at –20°C in single-use aliquots prior to use in epithelial cell cultures.

2D stromal cell culture

Primary E16 SMG stromal cells were cultured in 10 cm tissue culture dishes (Corning, 430167) containing 10 ml DMEM/F12+10% FBS+Pen-Strep with media replenished after plating and then every 2 days. Primary adult stromal cells were cultured in 35 mm tissue culture dishes (Corning, 353001) containing 2 ml DMEM/F12+10% FBS+Pen-Strep+50 ng/ml FGF2 with medium replaced every 3 days for 14–21 days until use in organoid preparations. All incubations were at 37°C with 5% CO₂ and cells were passaged when the density reached 90%. Cells were passaged and

isolated using standard trypsinization (Gibco, 25200056) techniques. For growth factor treatments, 50,000 SMG stromal cell (~0.2 glands’ worth of cells) at passage 1 were seeded on top of 50 mm glass bottom dishes (MatTek, P50G-1.5-14F) on day 0 and growth factors or pharmacological inhibitors were added from day 1 to 4.

Organoid epithelial and stromal cell isolation for transcriptomics

For organoid cultures, the media under the filter was replaced with 4°C FACS buffer, which was then replaced with FACS buffer on top of the organoids, which were incubated at 4°C for 20 min, triturated again, and collected into a 15 ml conical tube containing an equal volume of 4°C FACS buffer. The cells were triturated at 4°C to separate the cells and dissolve the Matrigel. Epithelial clusters were collected by centrifuging at 10× *g* for 1 min and resuspended in 4°C FACS buffer. Total RNA was extracted from these enriched epithelial cells for microarray analysis. Single stromal cells were pelleted at 450× *g* for 5 min and then resuspended in 4°C FACS buffer. The stroma was further negatively selected against epithelium using EPCAM antibody-coated microbeads (1:10; Miltenyi Biotec, 130-061-101) and a Miltenyi MS column. Either total RNA was extracted from the stromal cells for microarray analysis or the cells were used for scRNA-Seq.

RNA isolation for microarray and transcriptomic analysis

Total RNA was isolated using RNeasy mini kits (Qiagen, 74134) or RNAqueous micro kits (Thermo Fisher Scientific, AM1931). RNA quality was analyzed using a UV/Vis Spectrophotometer (NanoDrop ND-1000) at 260/280 nm and an Agilent 2100 Bioanalyzer. A 260–280 ratio of 1.7–2.2 and RIN score >7.0 were used as cut-offs, respectively. The RNA for transcriptome analyses were prepared with Clariom-S (Epithelium) (Thermo Fisher Scientific, 902930) or Clariom-D (Stroma) (Thermo Fisher Scientific, 902513) mouse microarrays. Data were analyzed using Transcriptome Analysis Console v.4.0.2.15, R functions and the Broad Institute’s GSEA software v4.

Immunocytochemistry and imaging

SMG organoid and cell cultures grown on Whatman Nuclepore filters (Cytiva, 110405) or glass coverslips were fixed with 4% PFA in 1×PBS for 20 min or in –20°C methanol for 18 min. Downstream antibody staining determined the fixation method. ICC was performed as described previously (Daley et al., 2009; Sequeira et al., 2012), with the use of 0.4% Triton-X 100 (Sigma, T9284-100ML) for PFA-fixed samples. All primary antibody incubations were overnight at 4°C. Secondary antibody incubations were for 1–3 h at room temperature. The primary antibodies and dilutions used were: AQP5 (1:400; Alomone, AQP-005), CNN1 (1:600; Abcam, ab46794), KRT7 (1:200; Abcam, ab9021), EPCAM-647 (1:400; Biolegend, 118212), PDGFR α (1:200; Thermo Fisher Scientific, 14-1401-81), PDGFR α (1:100; R&D Systems, AF1062-SP), PDGFR β (1:200; Abcam, ab32570), PDGFR β (1:100; Thermo Fisher Scientific, ab32570), HSPG2 (1:200; SantaCruz, sc-33707), α SMA/ACTA2 (1:1000; Sigma, 12-1402-81), THY1 (1:200; Biolegend, 105301), ENG (1:100; Thermo Fisher Scientific, 14-1051-81) and VIM (1:2000; Sigma, V2258). Secondary antibodies were Cyanine and Alexa dye-conjugated AffiniPure F(ab’)₂ fragments purchased from Jackson ImmunoResearch Laboratories and used at a dilution of 1:250. DAPI (1 μg/ml; Life Technologies, D1306) was used for nuclei staining together with secondary antibodies. Organoids were mounted on Whatman Nuclepore filters using antifade mounting media containing 90% (vol/vol) glycerol (Sigma, G5516-1L) in 1×PBS with 1–4 diazobicyclo[2,2,2]octane (Sigma, D27802-100G) and *n*-propyl gallate (Sigma, P3130-100G) as antifade agents (Gerdes et al., 2013; Valnes and Brandtzaeg, 1985). Imaging was performed using Zeiss Z1 Cell Observer widefield (for most experiments) or a Zeiss LSM 710 confocal or a Leica TCS SP5 confocal microscopes (for high-resolution imaging) at 10×, 20×, 40× and 63× (oil immersion) magnifications, with the same microscope and laser configurations for all samples within an experiment, as appropriate to the imaging method.

Quantification and statistical analyses

SEURAT v3.1.5 (Satija et al., 2015; Stuart et al., 2019) uses nonparametric Wilcoxon rank sum tests for statistical significance. Microarrays used RMA

normalization and log₂ transform in Transcriptome Analysis Console v4.0.2 (Thermo Fisher Scientific) or in R (R Core Team, 2021). Adjusted *P*-values of <0.05 and log fold change >1.99 were parameters used to determine differentially expressed genes. For ICC images, FIJI v1.53c performed the rolling-ball background subtraction and then color thresholding was used to calculate the stained area. To determine the staining area for organoid stromal measurements, regions of interest drawn by hand were used to include only stromal cells. To determine the staining area from organoid epithelial measurements, color thresholding on DAPI was used to select the more intensely DAPI-stained epithelial regions. For image quantification, at least one representative image was captured from each sample at a 5× widefield magnification that framed 20–40% of the entire sample. Statistical significance (*P*<0.05) was calculated between stained areas using a Student's *t*-test for dual-sample comparison or single-factor ANOVA followed with post-hoc Tukey HSD test for multisample comparisons. Statistical tests were performed in Microsoft Excel (Microsoft Corporation) or R. Staining area results are expressed as mean±standard deviation (s.d.).

Acknowledgements

The authors thank the University at Albany RNA Institute and Life Science Core facilities and the Center for Functional Genomics for equipment and expertise in both microarray and sequencing data creation. Specifically, Dr Sridar Chittur and Marcy Kuentzel.

Competing interests

The authors declare no competing or financial interests.

Author contributions

Conceptualization: N.M., D.A.N., M.L.; Methodology: N.M., A.M., D.A.N., A.L.A., M.L.; Software: N.M.; Validation: N.M.; Formal analysis: N.M., M.L.; Investigation: N.M., A.M., M.L.; Resources: P.F., M.L.; Data curation: N.M.; Writing - original draft: N.M.; Writing - review & editing: N.M., D.A.N., A.L.A., P.F., M.L.; Visualization: N.M.; Supervision: D.A.N., P.F., M.L.; Project administration: M.L.; Funding acquisition: P.F., M.L.

Funding

This work was supported by the National Institute of Dental and Craniofacial Research (R01DE027953 to M.L. and F31DE029688 to A.L.A.), the National Institute of Child Health and Human Development (R01HD097331-01 and 1R01DC017149-01A1 to P.F.) and by a University at Albany, SUNY Next Research Frontier Award to M.L. Deposited in PMC for release after 12 months.

Data availability

Raw data from scRNA-Seq and microarray studies have been deposited in GEO under SuperSeries GSE181430 or individually as GSE181425 (E16 stromal scRNA-Seq), GSE193041 (organoid scRNA-Seq), GSE181423 and GSE181424 (Clariom S and D microarrays, respectively). Scripts used to analyze data can be found on github (<https://github.com/MLarsenLab>).

Peer review history

The peer review history is available online at <https://journals.biologists.com/dev/article-lookup/doi/10.1242/dev.200167>.

References

- Avery, D., Govindaraju, P., Jacob, M., Todd, L., Monslow, J. and Puré, E. (2018). Extracellular matrix directs phenotypic heterogeneity of activated fibroblasts. *Matrix Biol.* **67**, 90–106. doi:10.1016/j.matbio.2017.12.003
- Bandyopadhyay, A., Tsuji, K., Cox, K., Harfe, B. D., Rosen, V. and Tabin, C. J. (2006). Genetic analysis of the roles of BMP2, BMP4, and BMP7 in limb patterning and skeletogenesis. *PLoS Genet.* **2**, 2116–2130. doi:10.1371/journal.pgen.0020216
- Bochaton-Piallat, M.-L., Gabbiani, G. and Hinz, B. (2016). The myofibroblast in wound healing and fibrosis: answered and unanswered questions. *F1000Research* **5**, 752. doi:10.12688/f1000research.8190.1
- Chatzeli, L., Gaete, M. and Tucker, A. S. (2017). Fgf10 and Sox9 are essential for the establishment of distal progenitor cells during mouse salivary gland development. *Development* **144**, 2294–2305. doi:10.1242/dev.146019
- Chatzeli, L., Teshima, T. H. N., Hajhosseini, M. K., Gaete, M., Proctor, G. B. and Tucker, A. S. (2021). Comparing development and regeneration in the submandibular gland highlights distinct mechanisms. *J. Anat.* **238**, 1371–1385. doi:10.1111/joa.13387

- Contreras, O., Cruz-Soca, M., Theret, M., Soliman, H., Tung, L. W., Groppa, E., Rossi, F. M. and Brandan, E. (2019). Cross-talk between TGF-β and PDGFRα signaling pathways regulates the fate of stromal fibro-adipogenic progenitors. *J. Cell Sci.* **132**, jcs232157. doi:10.1242/jcs.232157
- Daley, W. P., Gulfo, K. M., Sequeira, S. J. and Larsen, M. (2009). Identification of a mechanochemical checkpoint and negative feedback loop regulating branching morphogenesis. *Dev. Biol.* **336**, 169–182. doi:10.1016/j.ydbio.2009.09.037
- De Moerloose, L., Spencer-Dene, B., Revest, J., Hajhosseini, M., Rosewell, I. and Dickson, C. (2000). An important role for the IIIb isoform of fibroblast growth factor receptor 2 (FGFR2) in mesenchymal-epithelial signalling during mouse organogenesis. *Development* **127**, 483–492. doi:10.1242/dev.127.3.483
- Dominici, M., Le Blanc, K., Mueller, I., Slaper-Cortenbach, I., Marini, F., Krause, D., Deans, R., Keating, A., Prockop, D. and Horwitz, E. (2006). Minimal criteria for defining multipotent mesenchymal stromal cells. The International Society for Cellular Therapy position statement. *Cytotherapy* **8**, 315–317. doi:10.1080/14653240600855905
- Enge, M., Arda, H. E., Mignardi, M., Beausang, J., Bottino, R., Kim, S. K. and Quake, S. R. (2017). Single-cell analysis of human pancreas reveals transcriptional signatures of aging and somatic mutation patterns. *Cell* **171**, 321–330.e14. doi:10.1016/j.cell.2017.09.004
- Friedenstein, A. J., Chailakhjan, R. K. and Lalykina, K. S. (1970). The development of fibroblast colonies in monolayer cultures of guinea-pig bone marrow and spleen cells. *Cell and Tissue Kinetics* **3**, 393–403. doi:10.1111/j.1365-2184.1970.tb00347.x
- Gerdes, M. J., Sevinsky, C. J., Sood, A., Adak, S., Bello, M. O., Bordwell, A., Can, A., Corwin, A., Dinn, S., Filkins, R. J. et al. (2013). Highly multiplexed single-cell analysis of formalin-fixed, paraffin-embedded cancer tissue. *Proc. Natl. Acad. Sci. USA* **110**, 11982–11987. doi:10.1073/pnas.1300136110
- Hall, B. E., Zheng, C., Swaim, W. D., Cho, A., Nagineni, C. N., Eckhaus, M. A., Flanders, K. C., Ambudkar, I. S., Bruce, J. and Kulkarni, A. B. (2010). Conditional overexpression of TGF-β1 disrupts mouse salivary gland development and function. *Lab. Invest.* **90**, 543–555. doi:10.1038/labinvest.2010.5
- Hauser, B. R., Aure, M. H., Kelly, M. C., Hoffman, M. P. and Chibly, A. M. (2020). Generation of a single-cell RNAseq atlas of murine salivary gland development. *iScience* **23**, 101838. doi:10.1016/j.isci.2020.101838
- Hoffman, M. P., Kidder, B. L., Steinberg, Z. L., Lakhani, S., Ho, S., Kleinman, H. K. and Larsen, M. (2002). Gene expression profiles of mouse submandibular gland development: FGFR1 regulates branching morphogenesis in vitro through BMP- and FGF-dependent mechanisms. *Development* **129**, 5767–5778. doi:10.1242/dev.00172
- Hosseini, Z. F., Nelson, D. A., Moskwa, N., Sfakis, L. M., Castracane, J. and Larsen, M. (2018). FGF2-dependent mesenchyme and Laminin-111 are Niche factors in salivary gland organoids. *J. Cell Sci.* **131**, jcs208728. doi:10.1242/jcs.208728
- Hosseini, Z. F., Nelson, D. A., Moskwa, N. and Larsen, M. (2019). Generating embryonic salivary gland organoids. *Curr. Protoc. Cell Biol.* **83**, 1–20. doi:10.1002/cpcb.76
- Iwano, M., Plieth, D., Danoff, T. M., Xue, C., Okada, H. and Neilson, E. G. (2002). Evidence that fibroblasts derive from epithelium during tissue fibrosis. *J. Clin. Invest.* **110**, 341–350. doi:10.1172/JCI0215518
- Jaskoll, T. and Melnick, M. (1999). Submandibular gland morphogenesis: stage-specific expression of TGF-α/EGF, IGF, TGF-β, TNF, and IL-6 signal transduction in normal embryonic mice and the phenotypic effects of TGF-β2, TGF-β3, and EGF-r null mutations. *Anat. Rec.* **256**, 252–268. doi:10.1002/(SICI)1097-0185(19991101)256:3<252::AID-AR5>3.0.CO;2-6
- Jaskoll, T., Abichaker, G., Wtcher, D., Sala, F. G., Bellusci, S., Hajhosseini, M. K. and Melnick, M. (2005). FGF10/FGFR2b signaling plays essential roles during in vivo embryonic submandibular salivary gland morphogenesis. *BMC Dev. Biol.* **5**, 1–12. doi:10.1186/1471-213X-5-11
- Jensen, D. H., Oliveri, R. S., Trojahn Kølle, S.-F., Fischer-Nielsen, A., Specht, L., Bardow, A. and Buchwald, C. (2014). Mesenchymal stem cell therapy for salivary gland dysfunction and xerostomia: a systematic review of preclinical studies. *Oral Surgery, Oral Medicine, Oral Pathology Oral Radiology* **117**, 335–342.e1. doi:10.1016/j.oooo.2013.11.496
- Karpus, O. N., Westendorp, B. F., Vermeulen, J. L. M., Meisner, S., Koster, J., Muncan, V., Wildenberg, M. E. and van den Brink, G. R. (2019). Colonic CD90+ crypt fibroblasts secrete semaphorins to support epithelial growth. *Cell Rep.* **26**, 3698–3708.e5. doi:10.1016/j.celrep.2019.02.101
- Kinchen, J., Chen, H. H., Parikh, K., Antanaviciute, A., Jagielowicz, M., Fawcner-Corbett, D., Ashley, N., Cubitt, L., Mellado-Gomez, E., Attar, M. et al. (2018). Structural remodeling of the human colonic mesenchyme in inflammatory bowel disease. *Cell* **175**, 372–386.e17. doi:10.1016/j.cell.2018.08.067
- Kishi, J., Aono, Y., Sato, S., Koyama, K., Azuma, M., Abe, S., Kawano, H., Kishi, J., Toyoda, Y., Okazaki, H. et al. (2018). Blockade of platelet-derived growth factor receptor-β, not receptor-α ameliorates bleomycin-induced pulmonary fibrosis in mice. *PLoS ONE* **13**, 1–19. doi:10.1371/journal.pone.0209786

- Koslow, M., O'Keefe, K. J., Hosseini, Z. F., Nelson, D. A. and Larsen, M. (2019). ROCK inhibitor increases proacinar cells in adult salivary gland organoids. *Stem Cell Res.* **41**, 101608. doi:10.1016/j.scr.2019.101608
- Kramann, R., Schneider, R. K., Dirocco, D. P., Machado, F., Fleig, S., Bondzie, P. A., Henderson, J. M., Ebert, B. L. and Humphreys, B. D. (2015). Perivascular Gli1+ progenitors are key contributors to injury-induced organ fibrosis. *Cell Stem Cell* **16**, 51-66. doi:10.1016/j.stem.2014.11.004
- Krejci, P., Bryja, V., Pachernik, J., Hampl, A., Pogue, R., Mekikian, P. and Wilcox, W. R. (2004). FGF2 inhibits proliferation and alters the cartilage-like phenotype of RCS cells. *Exp. Cell Res.* **297**, 152-164. doi:10.1016/j.yexcr.2004.03.011
- Kuppe, C., Ibrahim, M. M., Kranz, J., Zhang, X., Ziegler, S., Perales-Patón, J., Jansen, J., Reimer, K. C., Smith, J. R., Dobie, R. et al. (2021). Decoding myofibroblast origins in human kidney fibrosis. *Nature* **589**, 281-286. doi:10.1038/s41586-020-2941-1
- Kusakabe, M., Sakakura, T., Sano, M. and Nishizuka, Y. (1985). A pituitary-salivary mixed gland induced by tissue recombination of embryonic pituitary epithelium and embryonic submandibular gland mesenchyme in mice. *Dev. Biol.* **110**, 382-391. doi:10.1016/0012-1606(85)90097-1
- Kwon, H. R., Nelson, D. A., DeSantis, K. A., Morrissey, J. M. and Larsen, M. (2017). Endothelial cell regulation of salivary gland epithelial patterning. *Development* **144**, 211-220. doi:10.1242/dev.142497
- Kwon, O.-J., Zhang, Y., Li, Y., Wei, X., Zhang, L., Chen, R., Creighton, C. J. and Xin, L. (2019). Functional heterogeneity of mouse prostate stromal cells revealed by single-cell RNA-seq. *iScience* **13**, 328-338. doi:10.1016/j.isci.2019.02.032
- Lee, J.-H., Tammela, T., Hoffee, M., Choi, J., Marjanovic, N. D., Han, S., Canner, D., Wu, K., Paschini, M., Bhang, D. H. et al. (2017). Anatomically and functionally distinct lung mesenchymal populations marked by Lgr5 and Lgr6. *Cell* **170**, 1149-1163.e12. doi:10.1016/j.cell.2017.07.028
- Li, R., Bernau, K., Sandbo, N., Gu, J., Preissl, S. and Sun, X. (2018). Pdgfra marks a cellular lineage with distinct contributions to myofibroblasts in lung maturation and injury response. *eLife* **7**, e36865. doi:10.7554/eLife.36865
- Liu, B., Dion, M. R., Jurasic, M. M., Gibson, G. and Jones, J. A. (2012). Xerostomia and salivary hypofunction in vulnerable elders: Prevalence and etiology. *Oral Surgery, Oral Medicine, Oral Pathology Oral Radiology* **114**, 52-60. doi:10.1016/j.oooo.2011.11.014
- Liu, J., Akanuma, N., Liu, C., Naji, A., Halff, G. A., Washburn, W. K., Sun, L. and Wang, P. (2016). TGF- β 1 promotes acinar to ductal metaplasia of human pancreatic acinar cells. *Sci. Rep.* **6**, 30904. doi:10.1038/srep30904
- Liu, N., Matsumura, H., Kato, T., Ichinose, S., Takada, A., Namiki, T., Asakawa, K., Morinaga, H., Mohri, Y., De Arcangelis, A. et al. (2019). Stem cell competition orchestrates skin homeostasis and ageing. *Nature* **568**, 344-350. doi:10.1038/s41586-019-1085-7
- Lombaert, I. M. A., Abrams, S. R., Li, L., Eswarakumar, V. P., Sethi, A. J., Witt, R. L. and Hoffman, M. P. (2013). Combined KIT and FGFR2b signaling regulates epithelial progenitor expansion during organogenesis. *Stem Cell Rep.* **1**, 604-619. doi:10.1016/j.stemcr.2013.10.013
- Lu, C. P., Polak, L., Keyes, B. E. and Fuchs, E. (2016). Spatiotemporal antagonism in mesenchymal-epithelial signaling in sweat versus hair fate decision. *Science* **354**, 1533. doi:10.1126/science.aah6102
- Macosko, E. Z., Basu, A., Satija, R., Nemes, J., Shekhar, K., Goldman, M., Tirosh, I., Bialas, A. R., Kamitaki, N., Martersteck, E. M. et al. (2015). Highly parallel genome-wide expression profiling of individual cells using nanoliter droplets. *Cell* **161**, 1202-1214. doi:10.1016/j.cell.2015.05.002
- Makarenkova, H. P., Hoffman, M. P., Beenken, A., Eliseenkova, A. V., Meech, R., Tsau, C., Patel, V. N., Lang, R. A. and Mohammadi, M. (2009). Differential interactions of FGFs with heparan sulfate control gradient formation and branching morphogenesis. *Sci. Signal.* **2**, ra55. doi:10.1126/scisignal.2000304
- Marmay, Y., Adar, R., Gaska, S., Wygoda, A., Maly, A., Cohen, J., Eliashar, R., Mizrachi, L., Orfaig-Geva, C., Baum, B. J. et al. (2016). Radiation-induced loss of salivary gland function is driven by cellular senescence and prevented by IL6 modulation. *Cancer Res.* **76**, 1170-1180. doi:10.1158/0008-5472.CAN-15-1671
- Martin, G. R. (1998). The roles of FGFs in the early development of vertebrate limbs. *Genes Dev.* **12**, 1571-1586. doi:10.1101/gad.12.11.1571
- McCarthy, N., Kraiczky, J. and Shivdasani, R. A. (2020a). Cellular and molecular architecture of the intestinal stem cell niche. *Nat. Cell Biol.* **22**, 1033-1041. doi:10.1038/s41556-020-0567-z
- McCarthy, N., Manieri, E., Storm, E. E., Saadatpour, A., Luoma, A. M., Kapoor, V. N., Madha, S., Gaynor, L. T., Cox, C., Keerthivasan, S. et al. (2020b). Distinct mesenchymal cell populations generate the essential intestinal BMP signaling gradient. *Cell Stem Cell* **26**, 391-402.e5. doi:10.1016/j.stem.2020.01.008
- Mizukoshi, K., Koyama, N., Hayashi, T., Zheng, L., Matsuura, S. and Kashimata, M. (2016). Shh/Ptch and EGF/ErbB cooperatively regulate branching morphogenesis of fetal mouse submandibular glands. *Dev. Biol.* **412**, 278-287. doi:10.1016/j.ydbio.2016.02.018
- Morikawa, S., Mabuchi, Y., Niibe, K., Suzuki, S., Nagoshi, N., Sunabori, T., Shimmura, S., Nagai, Y., Nakagawa, T., Okano, H. et al. (2009). Development of mesenchymal stem cells partially originate from the neural crest. *Biochem. Biophys. Res. Commun.* **379**, 1114-1119. doi:10.1016/j.bbrc.2009.01.031
- Nagaraju, C. K., Robinson, E. L., Abdesselem, M., Trenson, S., Dries, E., Gilbert, G., Janssens, S., Van Cleemput, J., Rega, F., Meyns, B. et al. (2019). Myofibroblast phenotype and reversibility of fibrosis in patients with end-stage heart failure. *J. Am. Coll. Cardiol.* **73**, 2267-2282. doi:10.1016/j.jacc.2019.02.049
- Neary, J. T., Kang, Y. and Shi, Y.-F. (2005). Cell cycle regulation of astrocytes by extracellular nucleotides and fibroblast growth factor-2. *Purinergic Signal.* **1**, 329-336. doi:10.1007/s11302-005-8075-y
- Nedvetsky, P. I., Emmerson, E., Finley, J. K., Ettinger, A., Cruz-Pacheco, N., Prochazka, J., Haddox, C. L., Northrup, E., Hodges, C., Mostov, K. E. et al. (2014). Parasympathetic innervation regulates tubulogenesis in the developing salivary gland. *Dev. Cell* **30**, 449-462. doi:10.1016/j.devcel.2014.06.012
- Ning, J., Zhao, Y., Ye, Y. and Yu, J. (2019). Opposing roles and potential antagonistic mechanism between TGF- β and BMP pathways: Implications for cancer progression. *EBioMedicine* **41**, 702-710. doi:10.1016/j.ebiom.2019.02.033
- Ó Hainmhire, E., Wu, H., Muto, Y., Donnelly, E. L., Machado, F. G., Fan, L. X., Chang-Panesso, M. and Humphreys, B. D. (2019). A conditionally immortalized Gli1-positive kidney mesenchymal cell line models myofibroblast transition. *Am. J. Physiol. Renal Physiol.* **316**, F63-F75. doi:10.1152/ajprenal.00460.2018
- Ohuchi, H., Hori, Y., Yamasaki, M., Harada, H., Sekine, K., Kato, S. and Itoh, N. (2000). FGF10 acts as a major ligand for FGF receptor 2 IIIb in mouse multi-organ development. *Biochem. Biophys. Res. Commun.* **277**, 643-649. doi:10.1006/bbrc.2000.3721
- Patel, V. N., Knox, S. M., Likar, K. M., Lathrop, C. A., Hossain, R., Eftekhari, S., Whitelock, J. M., Elkin, M., Vlodaevsky, I. and Hoffman, M. P. (2007). Heparanase cleavage of perlecan heparan sulfate modulates FGF10 activity during ex vivo submandibular gland branching morphogenesis. *Development (Cambridge, England)* **134**, 4177-4186. doi:10.1242/dev.011171
- Pedersen, A. M. L., Sørensen, C. E., Proctor, G. B., Carpenter, G. H. and Ekström, J. (2018). Salivary secretion in health and disease. *J. Oral Rehabil.* **45**, 730-746. doi:10.1111/joor.12664
- Plemons, J. M., Al-Hashimi, I. and Marek, C. L. (2014). Managing xerostomia and salivary gland hypofunction: executive summary of a report from the American Dental Association Council on Scientific Affairs. *J. Am. Dental Assoc.* **145**, 867-873. doi:10.14219/jada.2014.44
- Qiu, X., Mao, Q., Tang, Y., Wang, L., Chawla, R., Pliner, H. A. and Trapnell, C. (2017). Reversed graph embedding resolves complex single-cell trajectories. *Nat. Methods* **14**, 979-982. doi:10.1038/nmeth.4402
- R Core Team. (2021). *R: A Language and Environment for Statistical Computing*. R Foundation for Statistical Computing. <https://www.r-project.org/>
- Ramachandran, P., Dobie, R., Wilson-Kanamori, J. R., Dora, E. F., Henderson, B. E. P., Luu, N. T., Portman, J. R., Matchett, K. P., Brice, M., Marwick, J. A. et al. (2019). Resolving the fibrotic niche of human liver cirrhosis at single-cell level. *Nature* **575**, 512-518. doi:10.1038/s41586-019-1631-3
- Rastaldi, M. P., Ferrario, F., Giardino, L., Dell'Antonio, G., Grillo, C., Grillo, P., Strutz, F., Müller, G. A., Colasanti, G. and D'Amico, G. (2002). Epithelial-mesenchymal transition of tubular epithelial cells in human renal biopsies. *Kidney Int.* **62**, 137-146. doi:10.1046/j.1523-1755.2002.00430.x
- Rees, J. R. E., Onwuegbusi, B. A., Save, V. E., Alderson, D. and Fitzgerald, R. C. (2006). In vivo and in vitro evidence for transforming growth factor- β -mediated epithelial to mesenchymal transition in esophageal adenocarcinoma. *Cancer Res.* **66**, 9583-9590. doi:10.1158/0008-5472.CAN-06-1842
- Sakai, T., Larsen, M. and Yamada, K. M. (2003). Fibronectin requirement in branching morphogenesis. *Nature* **423**, 876-881. doi:10.1038/nature01712
- Sakakura, T., Nishizuka, Y. and Dawe, C. J. (1976). Mesenchyme-dependent morphogenesis and epithelium-specific cytodifferentiation in mouse mammary gland. *Science* **194**, 1439-1441. doi:10.1126/science.827022
- Sanchez-Duffhues, G., Williams, E., Goumans, M.-J., Heldin, C.-H. and ten Dijke, P. (2020). Bone morphogenetic protein receptors: Structure, function and targeting by selective small molecule kinase inhibitors. *Bone* **138**, 115472. doi:10.1016/j.bone.2020.115472
- Santini, M. P., Malide, D., Hoffman, G., Pandey, G., D'Escamard, V., Nomura-Kitabayashi, A., Rovira, I., Kataoka, H., Ochando, J., Harvey, R. P. et al. (2020). Tissue-resident PDGFR α + progenitor cells contribute to fibrosis versus healing in a context- and spatiotemporally dependent manner. *Cell Rep.* **30**, 555-570.e7. doi:10.1016/j.celrep.2019.12.045
- Satija, R., Farrell, J. A., Gennert, D., Schier, A. F. and Regev, A. (2015). Spatial reconstruction of single-cell gene expression data. *Nat. Biotechnol.* **33**, 495-502. doi:10.1038/nbt.3192
- Sekiguchi, R., Martin, D. and Yamada, K. M. (2020). Single-cell RNA-seq identifies cell diversity in embryonic salivary glands. *J. Dent. Res.* **99**, 69-78. doi:10.1177/0022034519883888
- Sequeira, S. J., Soscia, D. A., Oztan, B., Mosier, A. P., Jean-Gilles, R., Gadre, A., Cady, N. C., Yener, B., Castracane, J. and Larsen, M. (2012). The regulation of focal adhesion complex formation and salivary gland epithelial cell organization by nanofibrous PLGA scaffolds. *Biomaterials* **33**, 3175-3186. doi:10.1016/j.biomaterials.2012.01.010
- Shubin, A. D., Felong, T. J., Schutrum, B. E., Joe, D. S. L., Ovitt, C. E. and Benoit, D. S. W. (2017). Encapsulation of primary salivary gland cells in

- enzymatically degradable poly(ethylene glycol) hydrogels promotes acinar cell characteristics. *Acta Biomater.* **50**, 437-449. doi:10.1016/j.actbio.2016.12.049
- Song, E.-A. C., Min, S., Oyelakin, A., Smalley, K., Bard, J. E., Liao, L., Xu, J. and Romano, R. A.** (2018). Genetic and scRNA-seq analysis reveals distinct cell populations that contribute to salivary gland development and maintenance. *Sci. Rep.* **8**, 14043. doi:10.1038/s41598-018-32343-z
- Soriano, P.** (1997). The PDGF α receptor is required for neural crest cell development and for normal patterning of the somites. *Development* **124**, 2691-2700. doi:10.1242/dev.124.14.2691
- Steinberg, Z., Myers, C., Heim, V. M., Lathrop, C. A., Rebustini, I. T., Stewart, J. S., Larsen, M. and Hoffman, M. P.** (2005). FGFR2b signaling regulates ex vivo submandibular gland epithelial cell proliferation and branching morphogenesis. *Development (Cambridge, England)* **132**, 1223-1234. doi:10.1242/dev.01690
- Stuart, T., Butler, A., Hoffman, P., Hafemeister, C., Papalexi, E., Mauck, W. M., Hao, Y., Stoekius, M., Smibert, P. and Satija, R.** (2019). Comprehensive integration of single-cell data. *Cell* **177**, 1888-1902.e21. doi:10.1016/j.cell.2019.05.031
- Stzpeourginski, I., Nigro, G., Jacob, J.-M., Dulauroy, S., Sansonetti, P. J., Eberl, G. and Peduto, L.** (2017). CD34+mesenchymal cells are a major component of the intestinal stem cells niche at homeostasis and after injury. *Proc. Natl Acad. Sci. USA* **114**, 506-513. doi:10.1073/pnas.1620059114
- Subramanian, A., Tamayo, P., Mootha, V. K., Mukherjee, S., Ebert, B. L., Gillette, M. A., Paulovich, A., Pomeroy, S. L., Golub, T. R., Lander, E. S. et al.** (2005). Gene set enrichment analysis: A knowledge-based approach for interpreting genome-wide. *Proc. Natl. Acad. Sci. USA* **102**, 15545-15550. doi:10.1073/pnas.0506580102
- Takebe, T., Sekine, K., Enomura, M., Koike, H., Kimura, M., Ogaeri, T., Zhang, R.-R., Ueno, Y., Zheng, Y.-W., Koike, N. et al.** (2013). Vascularized and functional human liver from an iPSC-derived organ bud transplant. *Nature* **499**, 481-484. doi:10.1038/nature12271
- Takebe, T., Enomura, M., Yoshizawa, E., Kimura, M., Koike, H., Ueno, Y., Matsuzaki, T., Yamazaki, T., Toyohara, T., Osafune, K. et al.** (2015). Vascularized and complex organ buds from diverse tissues via mesenchymal cell-driven condensation. *Cell Stem Cell* **16**, 556-565. doi:10.1016/j.stem.2015.03.004
- Termén, S., Tan, E.-J., Heldin, C.-H. and Moustakas, A.** (2013). P53 regulates epithelial-mesenchymal transition induced by transforming growth factor B. *J. Cell. Physiol.* **228**, 801-813. doi:10.1002/jcp.24229
- Valnes, K. and Brandtzaeg, P.** (1985). Retardation of immunofluorescence fading during microscopy. *J. Histochem. Cytochem.* **33**, 755-761. doi:10.1177/33.8.3926864
- von Bültzingslöwen, I., Sollecito, T. P., Fox, P. C., Daniels, T., Jonsson, R., Lockhart, P. B., Wray, D., Brennan, M. T., Carrozzo, M., Gandera, B. et al.** (2007). Salivary dysfunction associated with systemic diseases: systematic review and clinical management recommendations. *Oral Surgery, Oral Medicine, Oral Pathology, Oral Radiology Endodontology* **103** Suppl., S57.e1-S57.e15. doi:10.1016/j.tripleo.2006.11.010
- Wang, S., Matsumoto, K., Lish, S. R., Cartagena-Rivera, A. X. and Yamada, K. M.** (2021). Budding epithelial morphogenesis driven by cell-matrix versus cell-cell adhesion. *Cell* **184**, 3702-3716.e30. doi:10.1016/j.cell.2021.05.015
- Wei, C., Larsen, M., Hoffman, M. P. and Yamada, K. M.** (2007). Self-organization and branching morphogenesis of primary salivary epithelial cells. *Tissue Eng.* **13**, 721-735. doi:10.1089/ten.2006.0123
- Wells, K. L., Gaete, M., Matalova, E., Deutsch, D., Rice, D. and Tucker, A. S.** (2013). Dynamic relationship of the epithelium and mesenchyme during salivary gland initiation: the role of Fgf10. *Biol. Open* **2**, 981-989. doi:10.1242/bio.20135306
- Weng, P.-L., Aure, M. H., Maruyama, T. and Ovitt, C. E.** (2018). Limited regeneration of adult salivary glands after severe injury involves cellular plasticity. *Cell Rep.* **24**, 1464-1470.e3. doi:10.1016/j.celrep.2018.07.016
- Woods, L. T., Camden, J. M., El-Sayed, F. G., Khalafalla, M. G., Petris, M. J., Erb, L. and Weisman, G. A.** (2015). Increased expression of TGF- β signaling components in a mouse model of fibrosis induced by submandibular gland duct ligation. *PLoS ONE* **10**, e0123641. doi:10.1371/journal.pone.0123641
- Yamamoto, S., Fukumoto, E., Yoshizaki, K., Iwamoto, T., Yamada, A., Tanaka, K., Suzuki, H., Aizawa, S., Arakaki, M., Yuasa, K. et al.** (2008). Platelet-derived growth factor receptor regulates salivary gland morphogenesis via fibroblast growth factor expression. *J. Biol. Chem.* **283**, 23139-23149. doi:10.1074/jbc.M710308200
- Yang, H., Adam, R. C., Ge, Y., Hua, Z. L. and Fuchs, E.** (2017). Epithelial-mesenchymal micro-niches govern stem cell lineage choices. *Cell* **169**, 483-496.e13. doi:10.1016/j.cell.2017.03.038
- Yoo, C., Vines, J. B., Alexander, G., Murdock, K., Hwang, P. and Jun, H.-W.** (2014). Adult stem cells and tissue engineering strategies for salivary gland regeneration: a review. *Biomaterials Res.* **18**, 1-12. doi:10.1186/2055-7124-18-9
- Yun, Y.-R., Won, J. E., Jeon, E., Lee, S., Kang, W., Jo, H., Jang, J.-H., Shin, U. S. and Kim, H.-W.** (2010). Fibroblast growth factors: Biology, function, and application for tissue regeneration. *J. Tissue Eng.* **1**, 1-18. doi:10.4061/2010/218142
- Zepp, J. A., Zacharias, W. J., Frank, D. B., Cavanaugh, C. A., Zhou, S., Morley, M. P. and Morrisey, E. E.** (2017). Distinct mesenchymal lineages and niches promote epithelial self-renewal and myofibrogenesis in the lung. *Cell* **170**, 1134-1148.e10. doi:10.1016/j.cell.2017.07.034
- Zepp, J. A., Morley, M. P., Loebel, C., Kremp, M. M., Chaudhry, F. N., Basil, M. C., Leach, J. P., Liberti, D. C., Niethamer, T. K., Ying, Y. et al.** (2021). Genomic, epigenomic, and biophysical cues controlling the emergence of the lung alveolus. *Science* **371**, eabc3172. doi:10.1126/science.abc3172
- Zhao, C., Cai, S., Shin, K., Lim, A., Kalisky, T., Lu, W.-J., Clarke, M. F. and Beachy, P. A.** (2017). Stromal *Gli2* activity coordinates a niche signaling program for mammary epithelial stem cells. *Science* **356**, eaal3485. doi:10.1126/science.aal3485
- Zhou, Y., Zhou, B., Pache, L., Chang, M., Khodabakhshi, A. H., Tanaseichuk, O., Benner, C. and Chanda, S. K.** (2019). Metascape provides a biologist-oriented resource for the analysis of systems-level datasets. *Nat. Commun.* **10**, 1523. doi:10.1038/s41467-019-09234-6